Electronic Supporting Information For

Environmentally Responsive Threading, Dethreading, and Fixation of Anion-induced Pseudorotaxanes

*Han-Yuan Gong, Brett M. Rambo, Elizabeth Karnas, Vincent M. Lynch, Karin M. Keller, and Jonathan L. Sessler**

Department of Chemistry & Biochemistry, The University of Texas at Austin, 1 University Station A5300, Austin, Texas, 78712-0165, USA

*e-mail: sessler@mail.utexas.edu

Materials and Method

Section S1: *General methods and compound labeling scheme (pp. S2-S4)*

Section S2: *NMR studies of the host-guest complexes of [**1**$^{4+}$·4PF_6^-] and 4,4'-biphenyldicarboxylate mono- and dianions (**6** and **7**) (pp. S5-S19)*

Section S3: *NMR studies of the host-guest complexes of [**1**$^{4+}$·4PF_6^-] and 2,6-naphthalenedicarboxylate mono- and dianions (**9** and **10**) (pp. S20-S32)*

Section S4: *Mass spectrometric studies of complexes* ***1***$^{4+}$ *with mono anions (****6*** *and* ***9****) as well as dianions (****4****,* ***7,*** *and* ***10****) (p. S33-S34)*

Section S5: *X-Ray crystallographic data (pp. S35-S43)*

Section S6: *Comparative analysis of pseudorotaxane complexes (pp. S44-S48)*

General Considerations: All solvents were dried before use according to standard procedures. For this study, deuterated solvents were purchased from Cambridge Isotope Laboratory (Andover, MA), and all other reagents were purchased commercially (Aldrich, Acros, or Fisher) and used without further purification. NMR spectroscopic studies were carried out using Varian Unity instruments (300 and 500 MHz). Chemical shifts (δ) are given in ppm and referenced to the residual solvent (^{1}H: DMSO-d_6 at 2.49 ppm). ESI-MS data was acquired by infusion on a Thermo LTQ-XL linear ion trap mass spectrometer operating in positive ion mode and the results are shown in Table S1.

All the crystals used to obtain X-ray diffraction structures grew as multiply intertwined colorless needles, colorless prisms, or other shapes as shown in Table S3 and the .cif documents corresponding to the specific structures in question. Diffraction grade crystals were obtained by slow evaporation from solution using a mixture of water/acetonitrile or water/acetonitrile/DMF as shown in Table S3.

The specific conditions used to obtain diffraction grade crystals were as follows: Solvent (DMF/acetonitrile/water, 1/1/1, v/v/v; 3 mL) was added to a mixture consisting of 0.120 mL of a 0.025 M solution of $\mathbf{1}^{4+}$ in acetonitrile, 0.120 mL of 0.1 M solution of $AgNO_3$ in water, and 0.120 mL of a 0.1 M solution of **3** in DMF. Upon addition of 0.1 mL triethylamine (TEA) a white solid precipitated from the clear solution. After filtering the precipitate, and allowing the clear solution to evaporate slowly, colorless prisms of $\mathbf{1}^{4+}\cdot(\mathbf{10})_3\cdot Ag_2\cdot 16\ H_2O$ were obtained after 4 weeks; these crystals proved suitable for an X-ray diffraction analysis.

The data crystals were cut from a cluster of crystals and had the approximate dimensions given in Table S3. The data was collected on a Nonius Kappa, Rigaku Mercury2 (2x2 bin mode) or Rigaku Saturn724+ (2x2 bin mode) CCD diffractometer using a graphite monochromator with MoKα radiation (λ = 0.71073 Å). The data was collected using ω-scans with a scan range of 1° at low temperature using an Oxford Cryostream low temperature device. Data reduction was performed using DENZO-SMN.[1] The structures were solved by direct methods using SIR97[2] and refined by full-matrix least-squares on F^2 with anisotropic displacement parameters for the non-H atoms using SHELXL-97.[3] The hydrogen atoms were calculated in ideal positions with isotropic displacement parameters set to 1.2xUeq of the attached atom (1.5xUeq for methyl hydrogen atoms). The refinement showed some typical warning signs of twinning. In particular, there were many reflections with large positive $\Delta(|F_o|^2 - |F_c|^2)$ values. The utility ROTAX[4] in the program WinGX[5] was used to look for possible twins. The $w(|Fo|^2 - |Fc|^2)^2$ function was minimized. Definitions used for calculating R(F), Rw(F2), and the quality of fit, S, are given in Table S3 and the .cif documents.[6] Neutral

atom scattering factors and values used to calculate the linear absorption coefficient are from the International Tables for X-ray Crystallography (1992).[7] All ellipsoid figures were generated using SHELXTL/PC.[8] Tables of positional and thermal parameters, bond lengths and angles, torsion angles, figures and lists of observed and calculated structure factors are located in the .cif documents available from the Cambridge Crystallographic Centre via quoting ref. numbers 775820, 775822, 775824 and 784454. These documents also contain details of crystal data, data collection, and structure refinement.

Compound Labeling Scheme for SI:

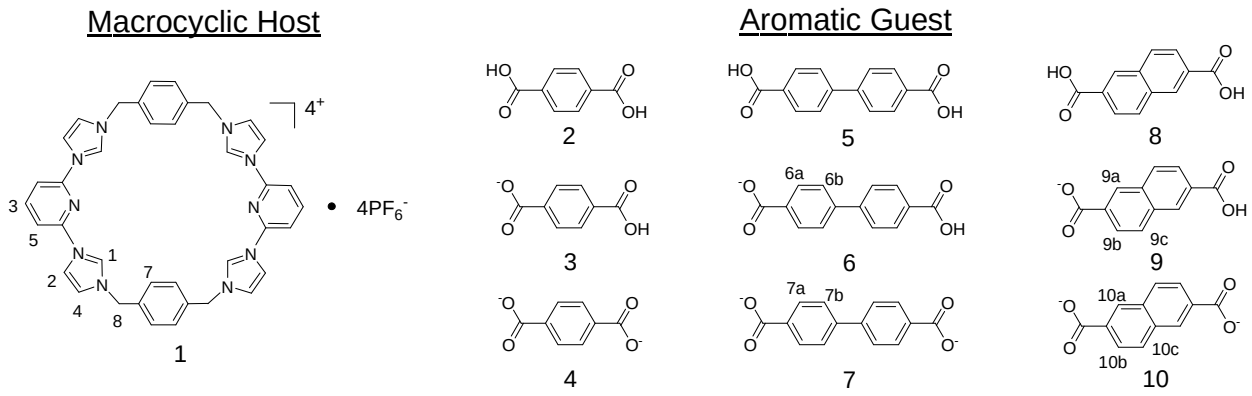

^{1}H NMR Studies of [1^{4+}•4PF_6^-] with guests 5 – 7

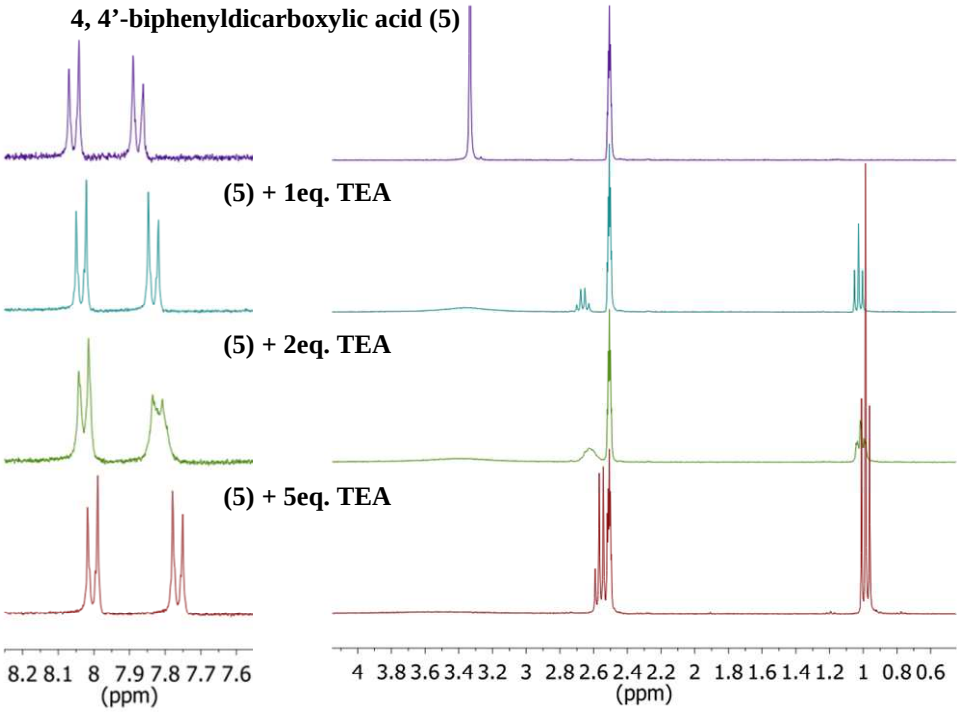

Figure S1. Expansion of the 300 MHz ^{1}H NMR spectra of 4,4'-biphenyldicarboxylic acid (*i.e.*, **5**; 5.00 × 10^{-3} M) recorded in the presence of 1, 2 and 5 molar equiv of triethylamine (TEA) in DMSO-d_6 at 300 K over the indicated spectral ranges.

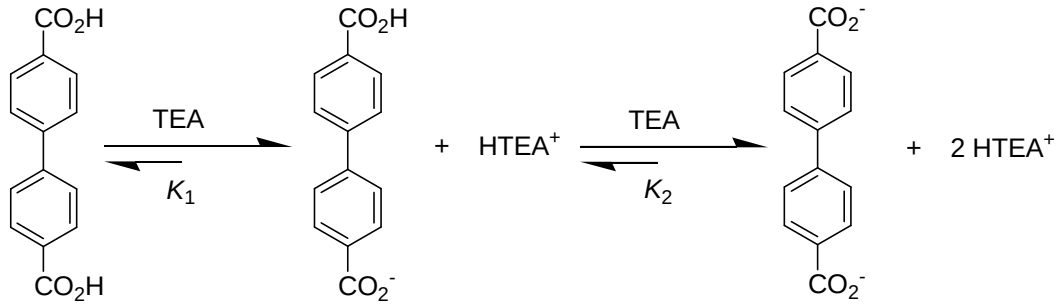

Scheme S1. The acid-base reaction between 4,4'-biphenyldicarboxylic acid (*i.e.*, **5**) and TEA**.**

In the equilibrium equation shown in Scheme S1, the equilibrium constants logK_1 and logK_2 are estimated to be 7.3 and 6.5, respectively.[9,10] Here, K_1 is greater than 10^7 M^{-1} and thus supports the dominant formation of the monoanion of 4,4'-biphenyldicarboxylic acid (*i.e.*, **6**) upon addition of 1 molar equiv TEA. The logK_2 value (6.5) supports the notion that addition of 5 equiv of TEA is sufficient for essentially complete deprotonation of **5**. These calculations and predictions are supported by the NMR spectra shown in Figure S1.

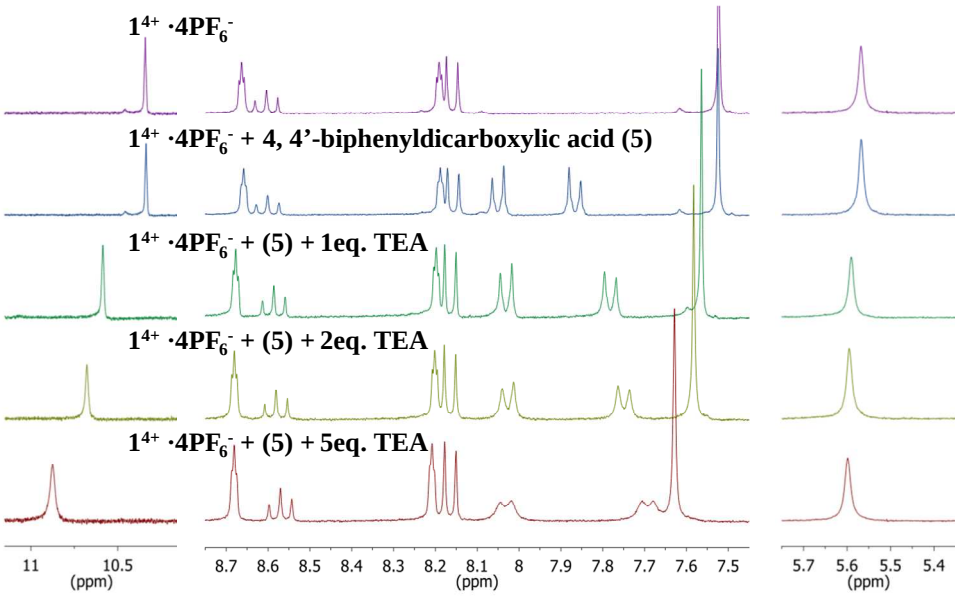

Figure S2. Expansion of the 300 MHz ^{1}H NMR spectrum of [$\mathbf{1}^{4+}\cdot 4PF_6^-$] ($5.00 \times 10^{-3}$ M) recorded in the presence of 1 equiv of **5**, and subsequent addition of 1, 2 and 5 molar equiv of TEA in DMSO-d_6 at 300 K over the indicated spectral ranges.

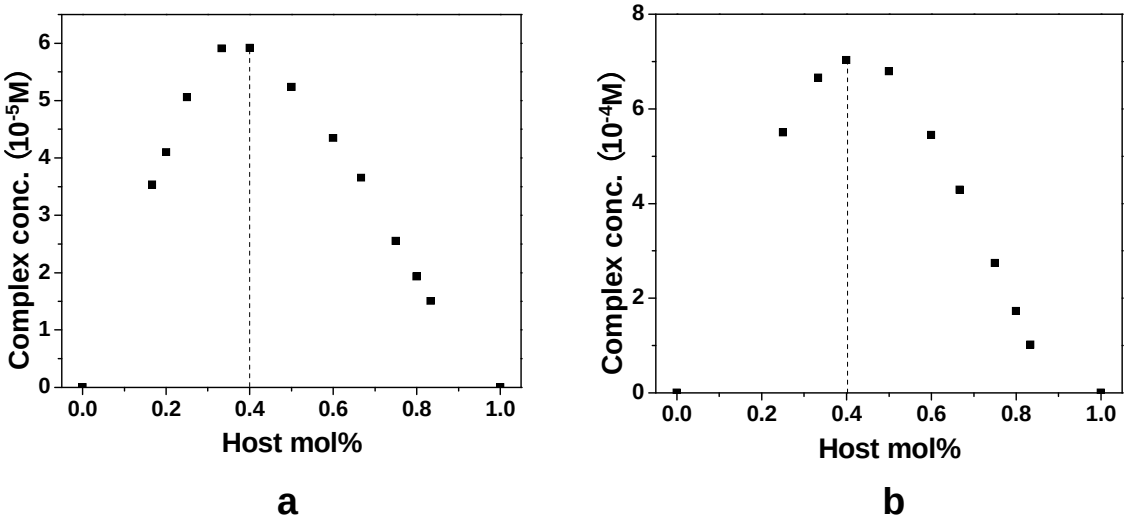

Figure S3. Job-plots corresponding to the binding between [$\mathbf{1}^{4+}\cdot 4PF_6^-$] and **6** constructed from 300 MHz ^{1}H NMR spectral data: (**a**) [host] + [guest] = 5×10^{-4} M and (**b**) [host] + [guest] = 5×10^{-3} M. The maximum values of both plots are at 0.4, a finding consistent with a 2:3 (host: guest) binding stoichiometry.[11]

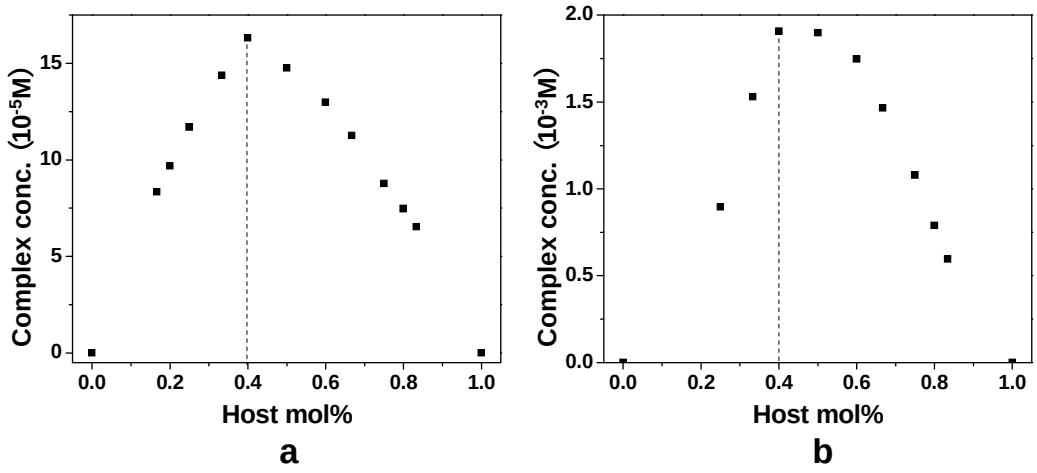

Figure S4. Job-plots corresponding to the binding between [$\mathbf{1}^{4+}\cdot 4PF_6^-$] and **7** constructed from 300 MHz ^{1}H NMR spectral data: (**a**) [host] + [guest] = 5×10^{-4} M and (**b**) [host] + [guest] = 5×10^{-3} M. The maximum values of both plots are at 0.4, a finding consistent with a 2:3 (host: guest) binding stoichiometry.[11]

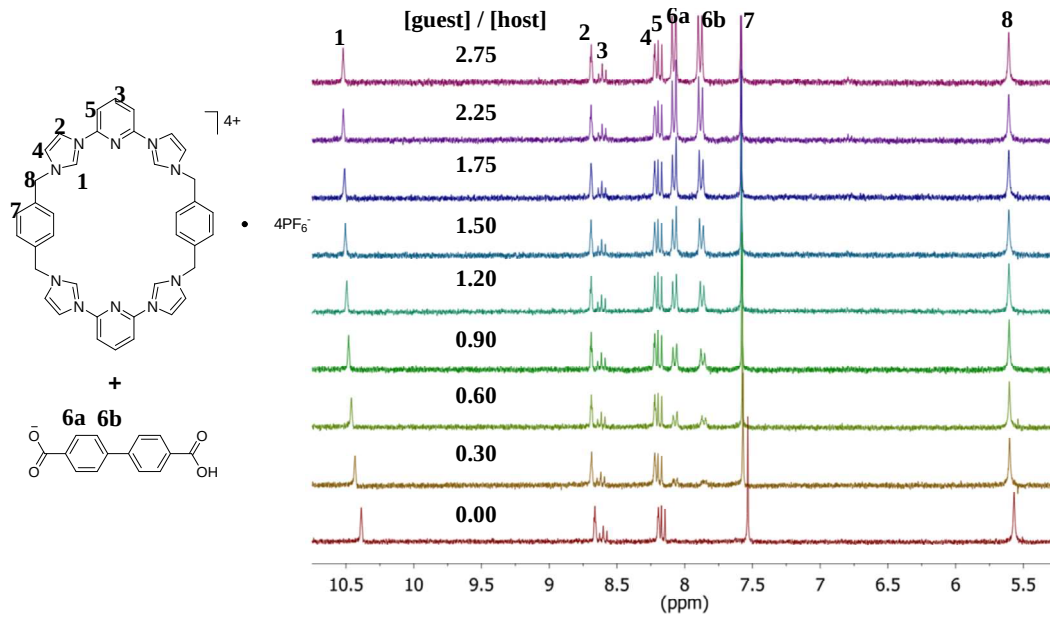

Figure S5. 300 MHz ^{1}H NMR spectroscopic titration of [$\mathbf{1}^{4+}\cdot 4PF_6^-$] ($5.00 \times 10^{-4}$ M) with **6** plus 1 equiv of TEA in DMSO-d_6 at 300 K.

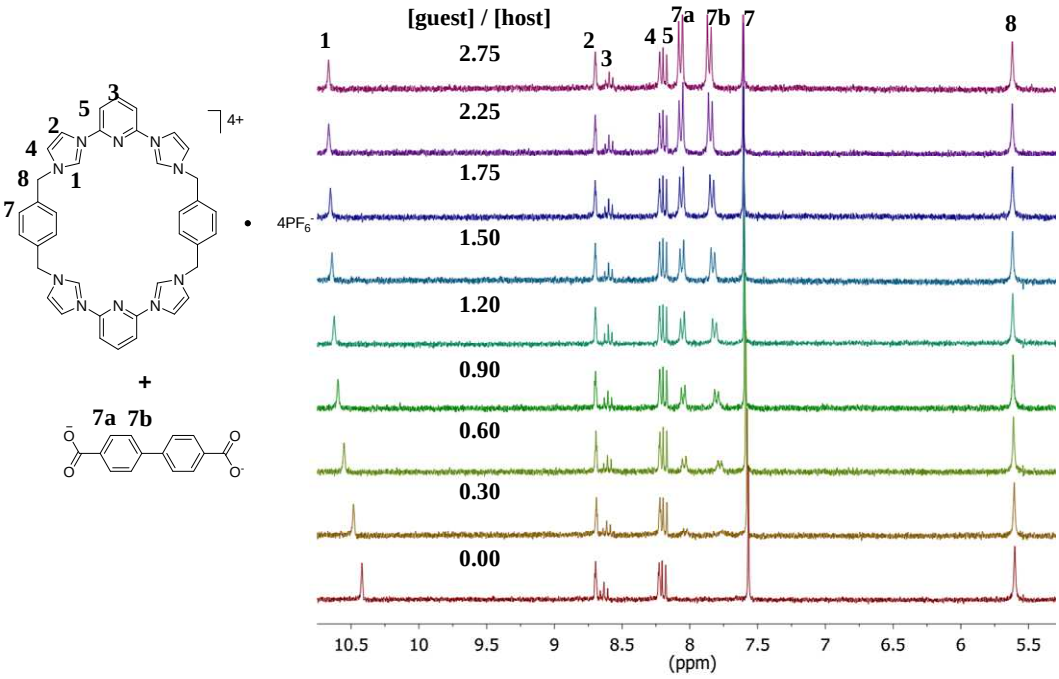

Figure S6. 300 MHz ^{1}H NMR spectroscopic titration of [$\mathbf{1}^{4+}\cdot 4PF_6^-$] ($5.0 \times 10^{-4}$ M) with **7** plus 5 molar equiv of TEA in DMSO-d_6 at 300 K.

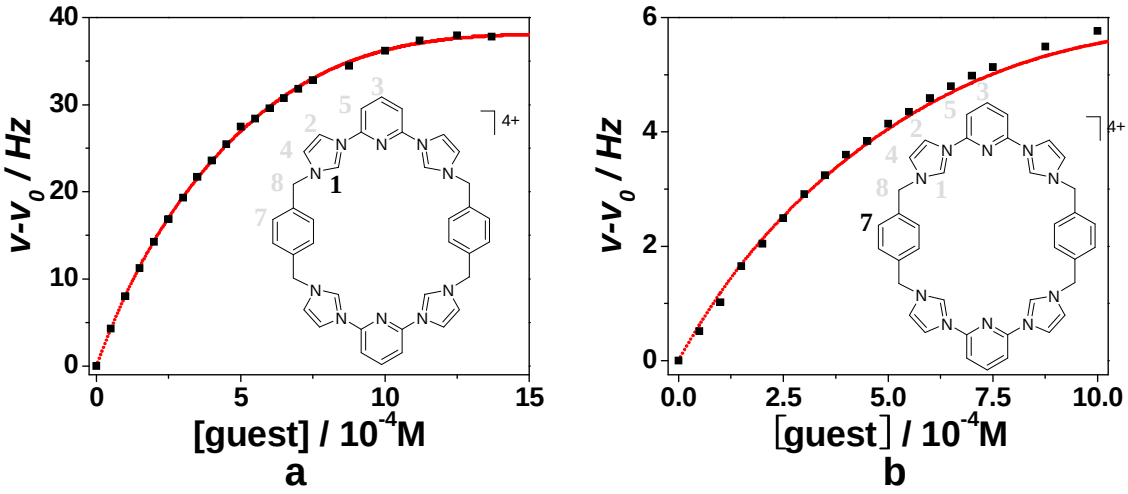

Figure S7. 300 MHz ^{1}H NMR binding isotherms corresponding to the interaction between [$\mathbf{1}^{4+}\cdot 4PF_6^-$] and **6** in DMSO-$d_6$ at 298 K. The chemical shift changes of (**a**) H(1) and (**b**) H(7) on $\mathbf{1}^{4+}$ were used to calculate K_1 ((1.5 ± 0.1) × 10^3 M^{-1}) and K_2 ((1.8 ± 0.2) × 10^7 M^{-2}) using the Hyperquad 2003 program.[12] The red dash lines show the non-linear curve for the calculated binding equation.

Even though it was not involved in the binding constants calculation, it was observed that the signal of H(3) shifts to high-field with the addition of the **6**. These changes provide evidence that the π-π donor-acceptor interactions are involved in the formation of a pseudorotaxane complex (i.e., [$\mathbf{1}^{4+}$•**6**]$^{3+}$) with the stoichiometry of 1:1 (host: guest). Alternatively, the peak associated with H(5) shifted to a lower field, and then shifted to higher field with the addition of excess guest anion species. This result leads us to suggest that excess anionic species can bind with the 1:1 complex (i.e., [$\mathbf{1}^{4+}$•**6**]$^{3+}$) and form a dimeric species with 2:3 (host: guest) ratio. We believe that the formation of such aggregates is primarily driven by anion···π donor-acceptor interactions (*cf.* Figure 1 in main text).

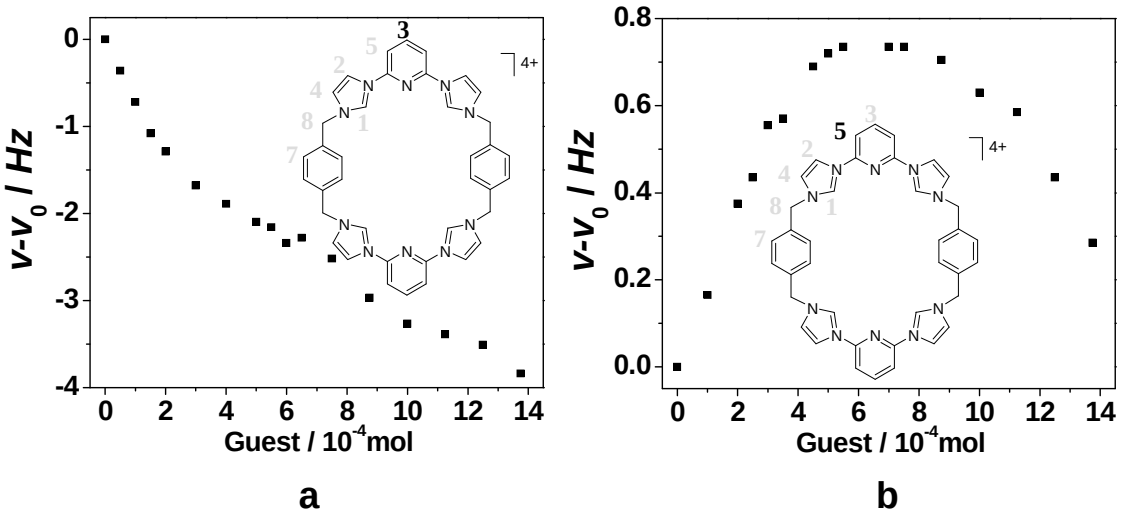

Figure S8. 300 MHz ^{1}H NMR binding isotherms corresponding to the interaction between [$\mathbf{1}^{4+}\cdot 4PF_6^-$] and **6** in DMSO-$d_6$ at 298 K. The chemical shift changes of (**a**) H(3) and (**b**) H(5) on $\mathbf{1}^{4+}$ were used for the binding mode analysis.

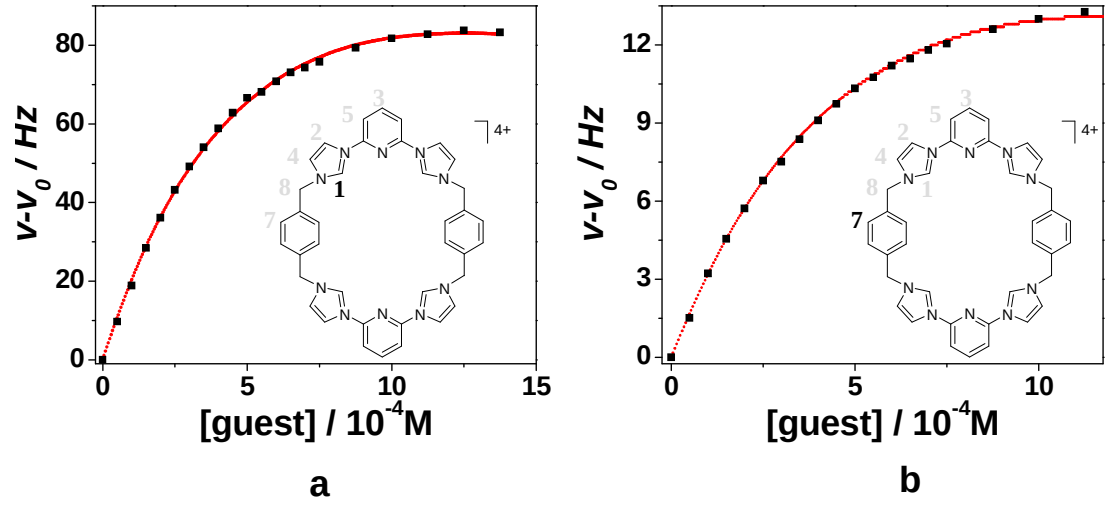

Figure S9. 300 MHz ^{1}H NMR binding isotherms associated with [$\mathbf{1}^{4+}\cdot 4PF_6^-$] and **7** in DMSO-$d_6$ at 298 K. The chemical shift changes of (**a**) H(1) and (**d**) H(7) on $\mathbf{1}^{4+}$ were used for the calculation of K_1 ($(1.8 \pm 0.2) \times 10^3$ M^{-1}) and K_2 ($(1.1 \pm 0.1) \times 10^7$ M^{-2}) using the Hyperquad 2003 program.[12] The red dash lines show the non-linear curve for the calculated binding equation.

The signals of H(3) and H(5) show similar changes upon addition of **7**. The binding isotherms in combination with Job Plot analysis provide evidence of a 1:1 pseudorotaxane complex (i.e., $[\mathbf{1}^{4+}\bullet 7]^{2+}$).

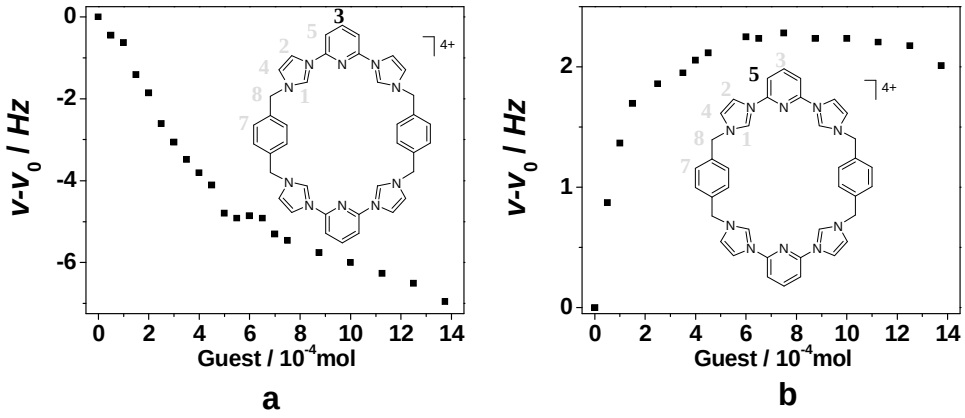

Figure S10. 300 MHz ^{1}H NMR binding isotherms corresponding to the interaction between $[\mathbf{1}^{4+}\cdot 4PF_6^-]$ and **7** in DMSO-d_6 at 298 K. The chemical shift changes of (**a**) H(3) and (**b**) H(5) on $\mathbf{1}^{4+}$ were used for the binding mode analysis.

NOESY spectroscopic studies were carried out in an effort to elucidate the nature of the host-guest interactions between macrocycle $\mathbf{1}^{4+}$ and **6** - **7** in solution.[13] Comparing the spectra of the complexes formed with **6** and **7** revealed that the similar binding modes are indeed involved. In both spectra, correlations between H(7) and H(6a), H(6b) (or H(7a), H(7b)) were observed; this is consistent with an "insert" binding mode (*i.e.* the anion "threading" into the core of macrocycle $\mathbf{1}^{4+}$ to form the pseudorotaxane structures).

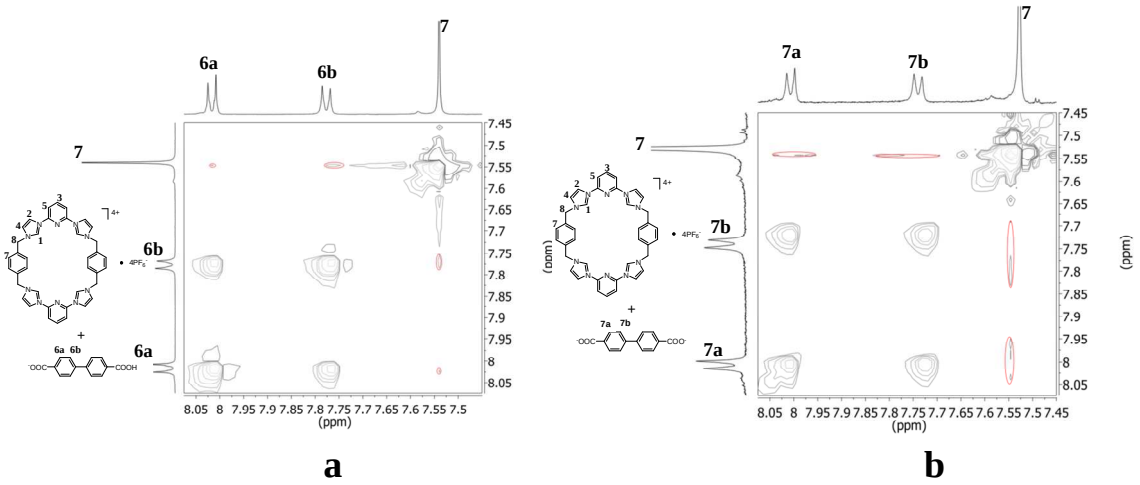

Figure S11. Expansion of the 500 MHz NOESY NMR spectra of [$\mathbf{1}^{4+}\cdot 4PF_6^-$] (5.00 mM) recorded in the presence of 1 molar equiv **6** (a) 1 molar equiv of **7** (b) in DMSO-d_6 at 300 K.

A concentration dependent ^{1}H NMR spectroscopic experiment was carried out for complex [$\mathbf{1}^{4+}$•**6**]$^{3+}$ (Figure 12).[14]

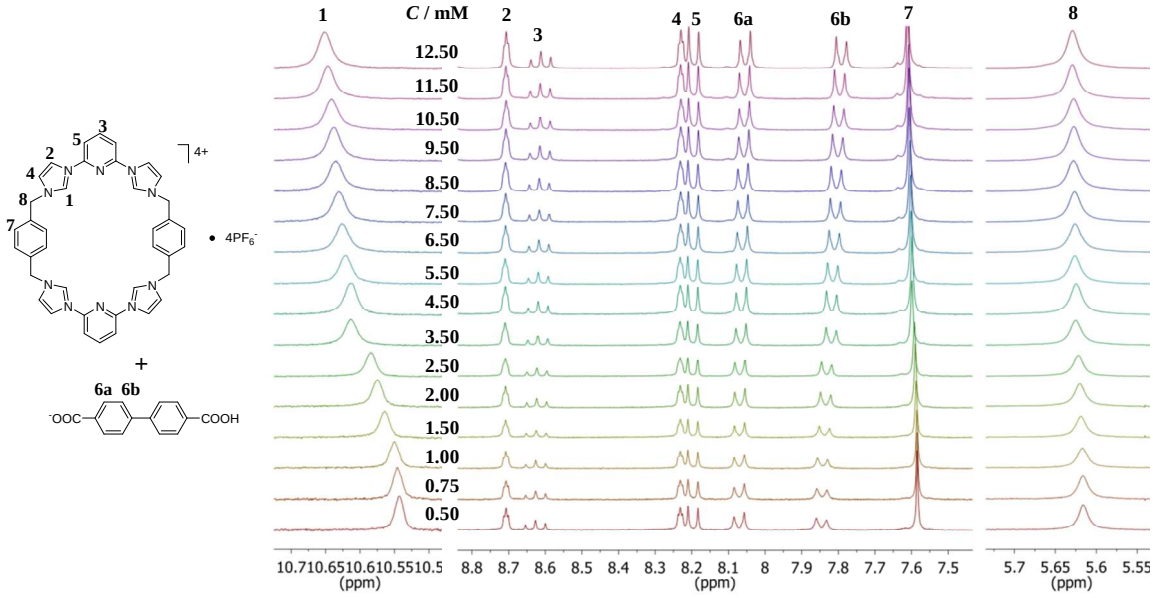

Figure S12. Concentration dependent 300 MHz ^{1}H NMR spectra recorded for [$\mathbf{1}^{4+}\cdot 4PF_6^-$] in the presence of 1 molar equiv of **6** in DMSO-d_6 at 300 K over the indicated spectral ranges**.**

Using the association constants K_1 and K_2 given in Figure S7, the difference of P_T (the detected NMR chemical shift) and P_C (the theoretical NMR shift; calculated) at various concentrations can be obtained, and from this the influence of $[\mathbf{1}^{4+}\cdot\mathbf{6}]^{3+}_n$ on the observed chemical shift can be extrapolated. Figure S12 (*vide supra*) shows a concentration dependant NMR study carried out with $[\mathbf{1}^{4+}\cdot\mathbf{6}]^{3+}_n$, and from this we observe that P_T and P_C fit well each other. This observation leads us to suggest that no oligomeric structures are observed in solution when the solution concentration of $[\mathbf{1}^{4+}\cdot\mathbf{6}]^{3+}$ is increased.

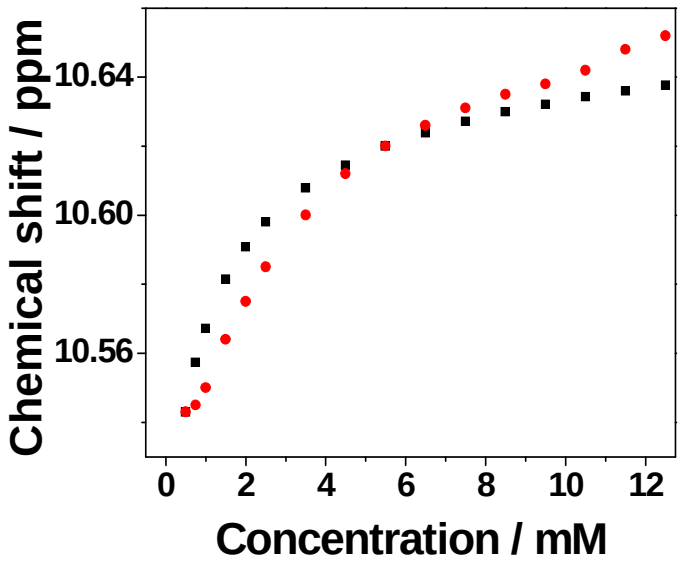

Figure S13. Calculated shift (P_T (■)) and observed shift (P_C (●)) obtained while monitoring H(1) using 300 MHz ^{1}H NMR of a solution of $[\mathbf{1}^{4+}\cdot 4PF_6^-]$ and 1 molar equiv of **6** in DMSO-d_6; the overall solution concentration was incrementally increased.

Temperature dependent NMR spectra were used to obtain further insights into the complex formation and the self-association processes (Figures S14, 15 and 16).[16]

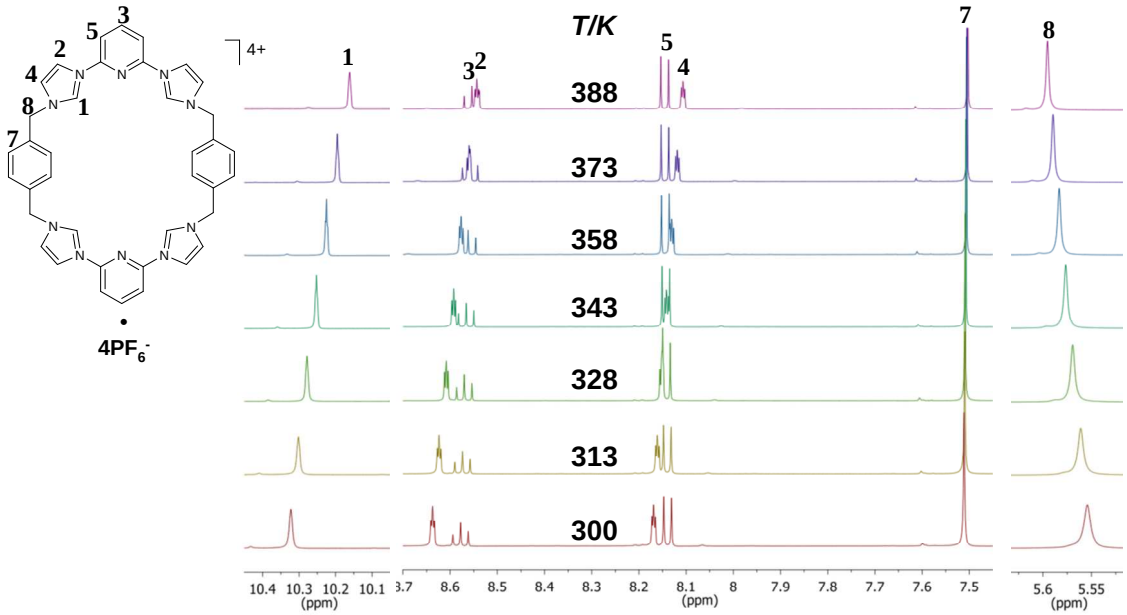

Figure S14. Expansion of the temperature dependent 500 MHz ^{1}H NMR spectra of [$\mathbf{1}^{4+}\cdot 4PF_6^-$] ($1.25 \times 10^{-2}$ M) in DMSO-d_6 over the indicated spectral ranges.

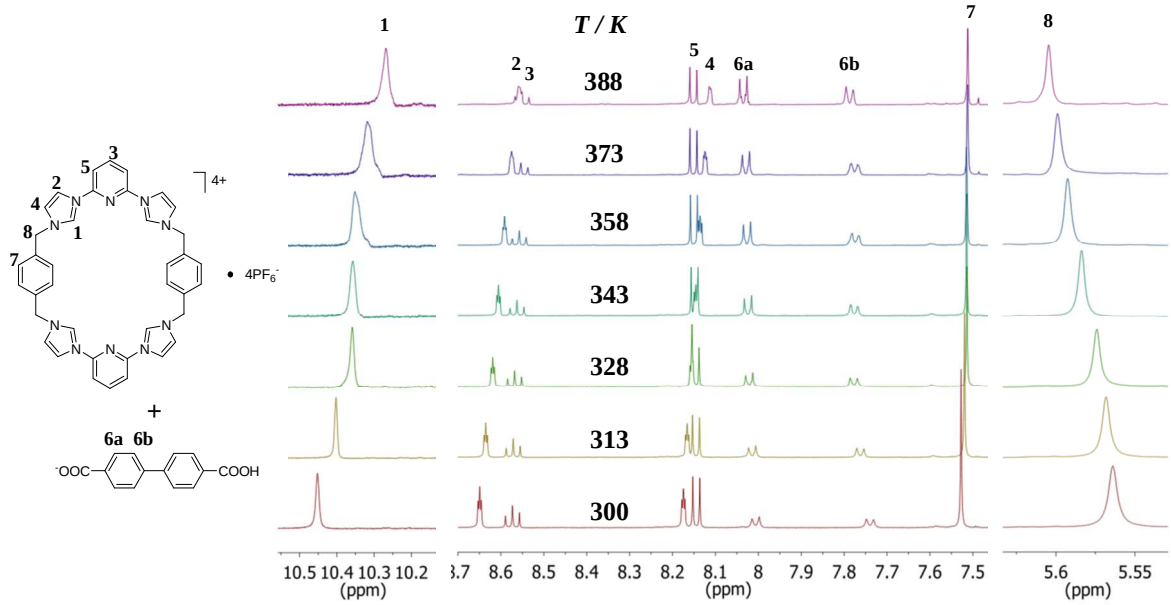

Figure S15. Expansion of the temperature dependent 500 MHz ^{1}H NMR spectra of [$\mathbf{1}^{4+}\cdot 4PF_6^-$] ($5.00 \times 10^{-3}$ M) in the presence of 1 molar equiv of **6** in DMSO-d_6 over the indicated spectral ranges.

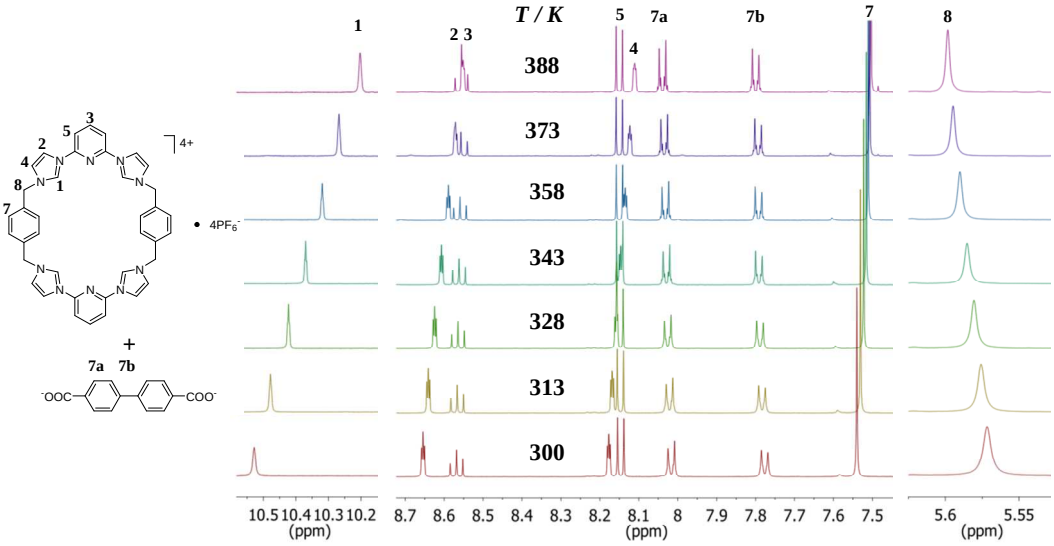

Figure S16. Expansion of the temperature dependent 500 MHz ^{1}H NMR spectra of [$\mathbf{1}^{4+}\cdot 4PF_6^-$] (5.00 × 10^{-3} M) in the presence of 1 molar equiv. of **7** in DMSO-d_6 over the indicated spectral ranges.

Temperature dependent ^{1}H NMR studies (*vide supra*) provide evidence that as the solution temperature is increased the respective pseudorotaxane complexes begin to disassociate. The dethreading of the pseudrotaxane complexes was determined, in this case, by monitoring H(1) on macrocycle $\mathbf{1}^{4+}$. Distinct chemical shifts of the signal associated with H(1) was observed via ^{1}H NMR solution studies containing [$\mathbf{1}^{4+}\cdot\mathbf{6}]^{3+}$ and [$\mathbf{1}^{4+}\cdot 7]^{2+}$ as the temperature was increased from 300 K to 388 K. Complexes [$\mathbf{1}^{4+}\cdot\mathbf{6}]^{3+}$ and [$\mathbf{1}^{4+}\cdot 7]^{2+}$ both show a similar rate of change between 300 K and 328 K. However, when the temperature was increased between the range of 328K and 358K, complex [$\mathbf{1}^{4+}\cdot\mathbf{7}]^{2+}$ appears to dethread at an accelerated rate (as compared to [$\mathbf{1}^{4+}\cdot\mathbf{6}]^{3+}$). It was observed that when the temperature was above 358K both complexes begin to deaggregate, but complex [$\mathbf{1}^{4+}\cdot\mathbf{7}]^{2+}$ displays an overall larger chemical shift (monitoring H(1)) than is observed with complex [$\mathbf{1}^{4+}\cdot\mathbf{6}]^{3+}$). This result leads us to suggest that the binding interactions and overall binding mode of [$\mathbf{1}^{4+}\cdot\mathbf{6}]^{3+}$ is different than what is observed for [$\mathbf{1}^{4+}\cdot\mathbf{7}]^{2+}$ (*vide infra*).

The temperature dependant NMR spectral data (shown in Figure S15 and S16) was also utilized to gain a better understanding of the binding mode observed in the formation of the pseudorotaxane complexes (Figure S17). In complex $[\mathbf{1}^{4+}\cdot\mathbf{6}]^{3+}$ a distinct lower-field shift of the signal associated with H(1) observed as the temperature is increased from 300 K to 328 K leading us to suggest that this structural complex is dominated by C-H···anion interactions at lower temperature. Further, a slight higher-field chemical shift was observed in the signal corresponding to H(1) of $\mathbf{1}^{4+}$ when the temperature was increased between 328 K and 360 K supporting the notion that binding mode changes to what is predominantly π···π interaction. This type of molecular bonding interaction is typically not as sensitive to temperature change as their hydrogen bonding counterparts. In contrast, complex $[\mathbf{1}^{4+}\cdot\mathbf{7}]^{2+}$ appears to predominantly consist of C-H···anion binding interactions over the full temperature range.

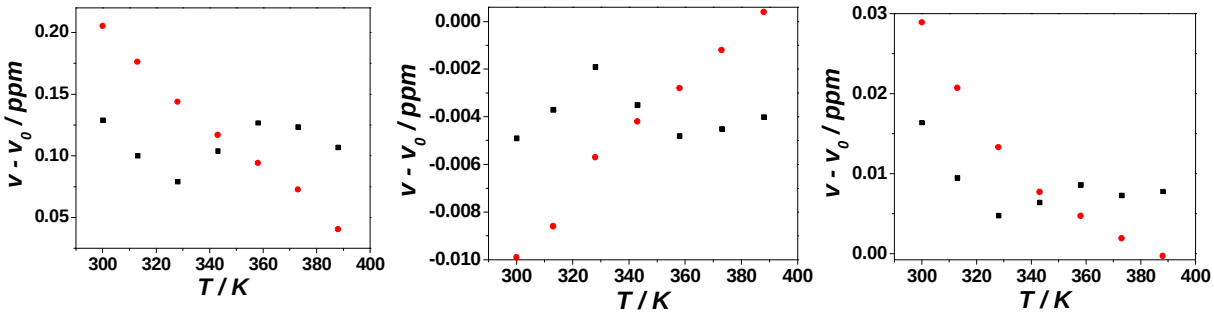

Figure S17. 500 MHz ^{1}H NMR chemical shifts for (**a**) H(1), (**b**) H(3) and (**c**) H(7) of $\mathbf{1}^{4+}\cdot 4PF_6^-$ (5.00 mM) recorded in the presence of 1 molar equiv of varying guest anions in DMSO-d_6 at different temperatures. Here, "■" represents $[\mathbf{1}^{4+}\cdot 4PF_6^-]$ in the presence of 1 molar equiv of **6**; "●" represents $[\mathbf{1}^{4+}\cdot 4PF_6^-]$ in the presence of 1 molar equiv of **7**.

Next, the effects of pH on pseudorotaxane formation were investigated. Initially, TEA was added to a DMSO-d_6 solution contining $\mathbf{1}^{4+}$ (2.00 mM) and 1 molar equiv of diacid **5.** This resulted in higher-field shift in the signals associated with H(1) and H(7) (Figure S18) leading us to suggest that pseudorotaxane formation was effectively "turned on" by

converting the guest species to dianion **7**. Subsequently, the solution was acidified by adding excess deuterium TFA (i.e., deuterium trifluoroacetic acid, CF_3COOD) which resulted in a lower-field field shift of the signals associated with H(1) and H(7). This leads us to suggest that addition of acid was sufficient in neutralizing dianion **7** effectively converting it back to diacid **5,** which resulted in a dethreading or "turning off" the pseudorotaxane complex. These cycles could be repeated as shown in Figure S19. However, a dampening of the frequency was observed as the repetitions increased. Here we postulate that this result reflects strong buffering capabilities of the $H(D)TEA^+$-CF_3COO^- solution (*cf.* Figure 21).

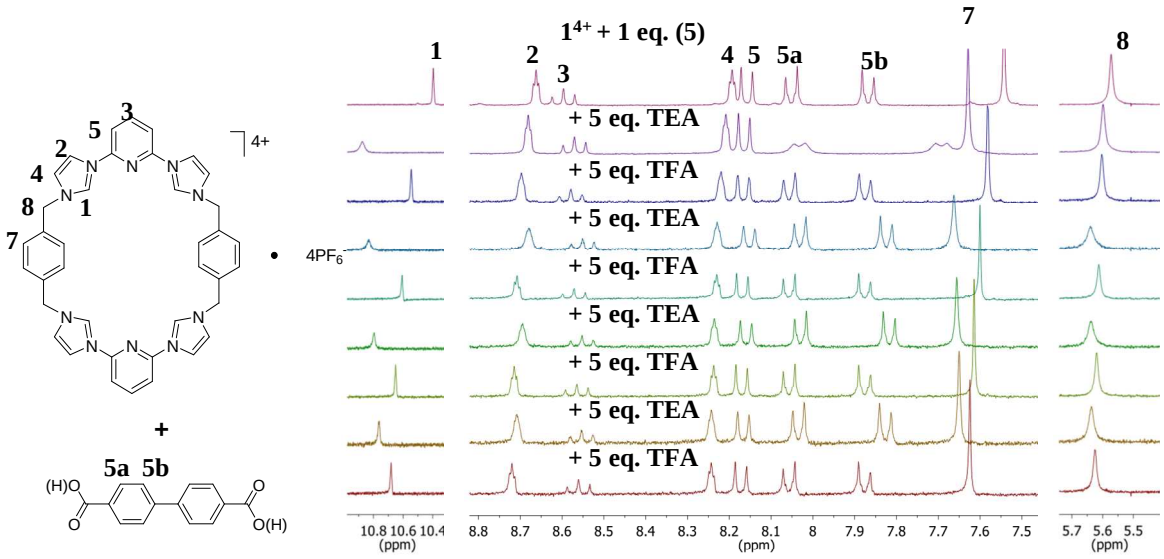

Figure S18. Cycling of the switch as observed by measurement of the 300 MHz ^{1}H NMR spectra at 300 K in DMSO-d_6. The concentration of $\mathbf{1}^{4+}$ has been maintained as 2.00 mM with 1 molar equiv. **5**. The first and later cycles were produced by alternating addition of 5 molar equiv. TEA and 5 molar equiv. CF_3COOD.

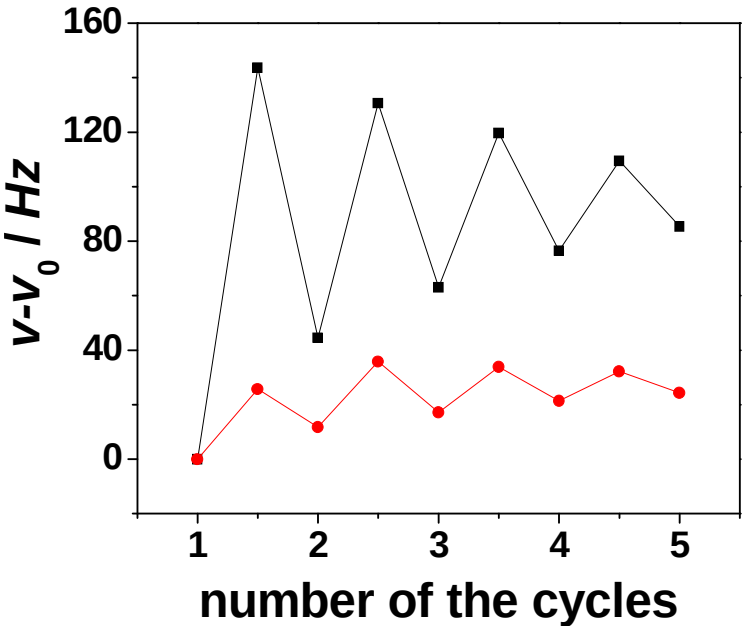

Figure S19. Cycles of pseudorotaxane threading and dethreading as determined by changes in the chemical shift of the 300 MHz ^{1}H NMR signals associated with H(1) (represented as "■") and H(7) (represented as "●") on $\mathbf{1}^{4+}$ at 300 K in DMSO-d_6. The initial concentration of $\mathbf{1}^{4+}$ was maintained throughout the study at 2.00 mM with 1 molar equiv **5**. The first step in each cycle is the addition of 5 molar equiv TEA and the second is the addition of 5 molar equiv CF_3COOD.

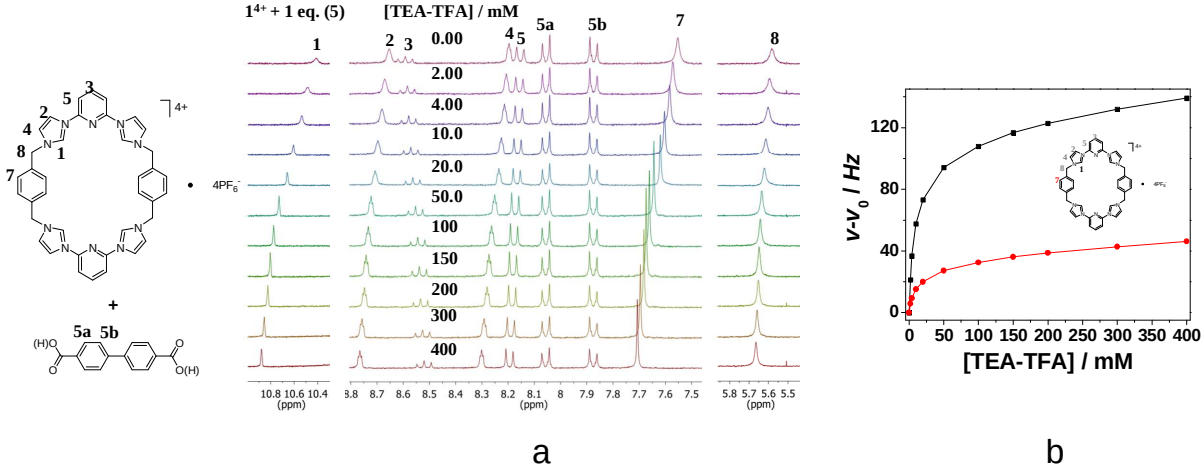

Figure S20. 300 MHz ^{1}H NMR spectroscopic titration of a solution containing [$\mathbf{1}^{4+}\cdot 4PF_6^-$] ($2.0 \times 10^{-3}$ M) and 1 molar equiv **5** via the addition of H(D)TEA$^+$-CF_3COO^- (TEA-TFA)

salt in DMSO-d_6 at 300 K. (a) The ^{1}H NMR spectra and (b) the chemical shift change of the signal associated with H(1) (represented as "■") and H(7) (represented as "●") on $\mathbf{1}^{4+}$ during the titration.

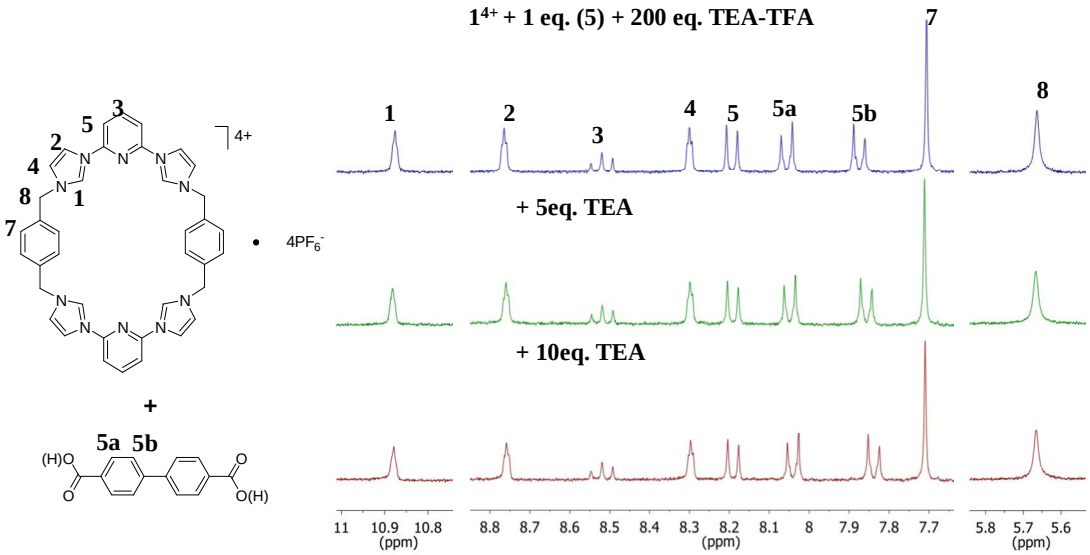

Figure S21. Expansion of the 300 MHz ^{1}H NMR spectra of [$\mathbf{1}^{4+}\cdot 4PF_6^-$] ($2.00 \times 10^{-3}$M) and 1 molar equiv **5** recorded in the presence of 200 molar equiv of H(D)TEA$^+$-CF_3COO^- (TEA-TFA) salt, and subsequent addition of 0, 5 and 10 molar equiv of TEA in DMSO-d_6 at 300 K over the indicated spectral ranges. The similarity in these spectra demonstrates the strong buffer capabilities of H(D)TEA$^+$-CF_3COO^- solution at high concentrations.

^{1}H NMR Studies of [1^{4+}•4PF_6^-] with guests 8 – 10

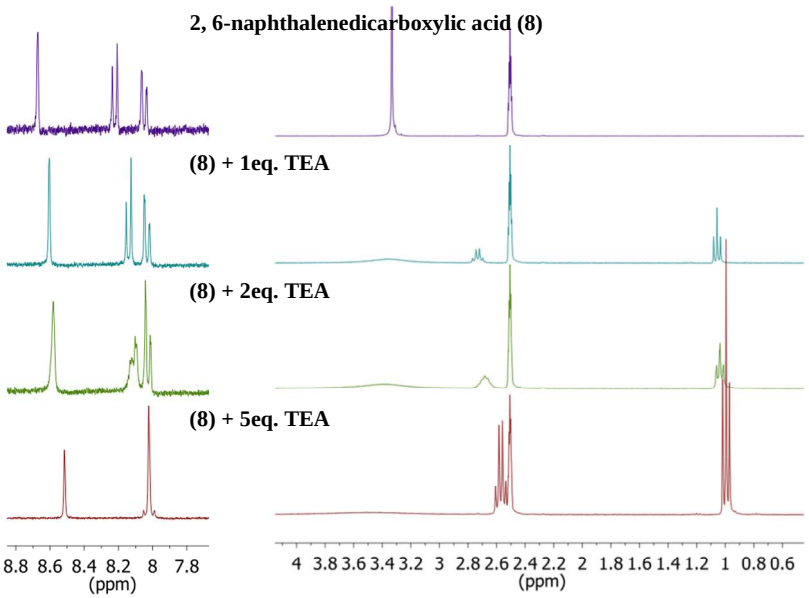

Figure S22. Expansion of the 300 MHz ^{1}H NMR spectra of 2,6-naphthalenedicarboxylic acid (*i.e.*, **8**; 5.00 × 10^{-3} M) recorded in the presence of 1, 2 and 5 molar equiv of triethylamine (TEA) in DMSO-d_6 at 300 K over the indicated spectral ranges.

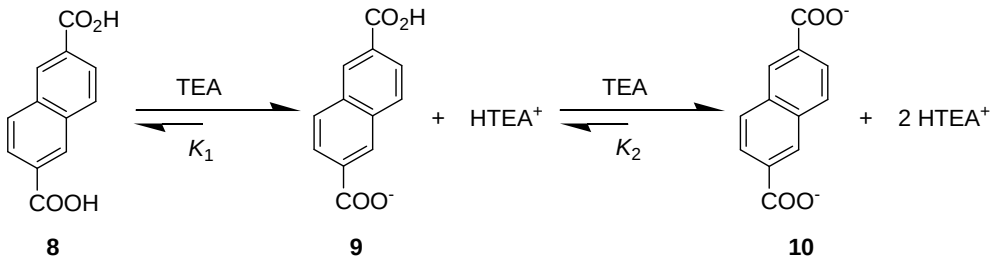

Scheme S2. The acid-base reaction between **8** and TEA.

In the equilibrium equation shown in Scheme S2, the equilibrium constants logK_1 and log K_2 are estimated to be 7.0 and 6.1, respectively.[9,15] The K_1 value is as great as 10^7 M^{-1} and thus supports the dominant formation of **9** upon addition of 1 molar equiv TEA. The logK_2 value of 6.1 supports the notion that addition of 5 equiv of TEA is sufficient for essentially

complete deprotonation of **8** and subsequent conversion to **10**. These calculations and predictions are supported by the NMR spectra shown in Figure S22.

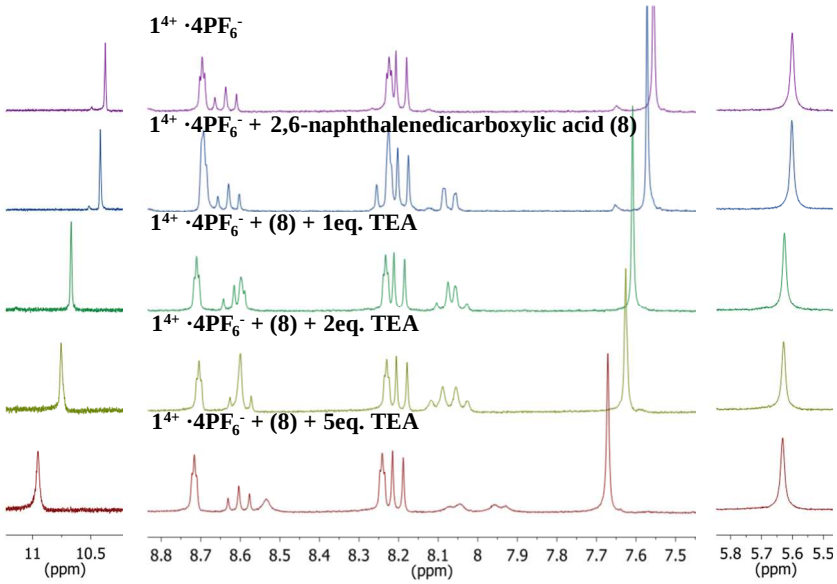

Figure S23. Expansion of the 300 MHz ^{1}H NMR spectrum of [$\mathbf{1}^{4+}\cdot 4PF_6^-$] ($5.00 \times 10^{-3}$ M) recorded in the presence of 1 equiv **8** and upon addition of 1, 2 and 5 molar equiv. of TEA in DMSO-d_6 at 300 K over the indicated spectral ranges.

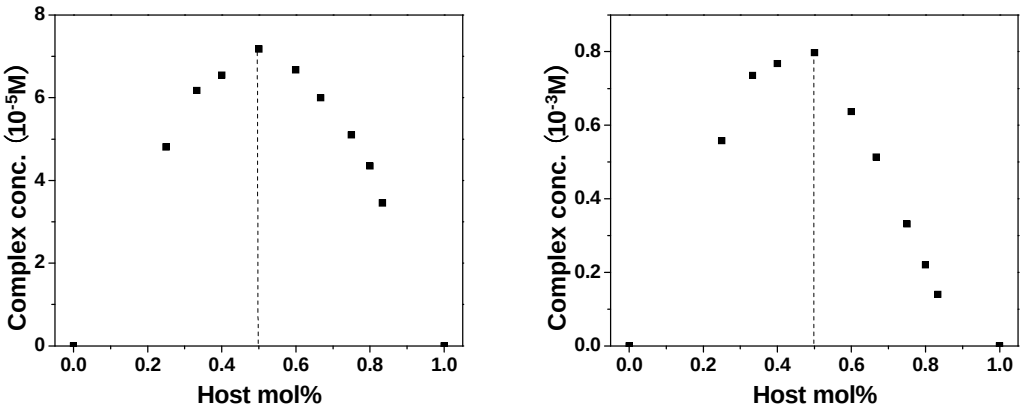

Figure S24. Job-plots corresponding to the binding between [$\mathbf{1}^{4+}\cdot 4PF_6^-$] and **9** constructed from 300 MHz ^{1}H NMR spectral data. (**a**) [host] + [guest] = 5×10^{-4} M and (**b**) [host] + [guest] = 5×10^{-3} M. The maximum values of both Job-plots displayed maximum values at 0.5 These findings are consistent with a 1:1 (host:guest) binding stoichiometry.[11]

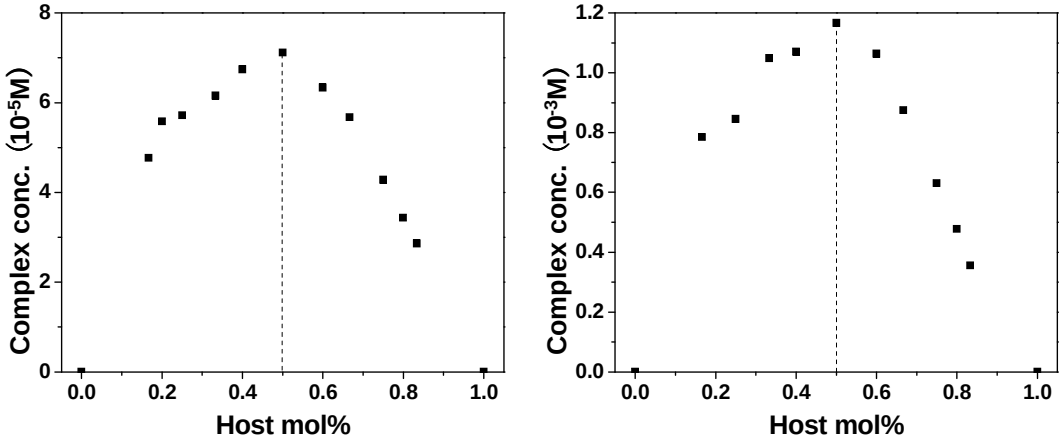

Figure S25. Job-plots corresponding to the binding between [$\mathbf{1}^{4+}\cdot 4PF_6^-$] and **10** constructed from 300 MHz ^{1}H NMR spectral data. (**a**) [host] + [guest] = 5×10^{-4} M and (**b**) [host] + [guest] = 5×10^{-3} M. The maximum values of both Job-plots displayed maximum values at 0.5 These findings are consistent with a 1:1 (host:guest) binding stoichiometry.[11]

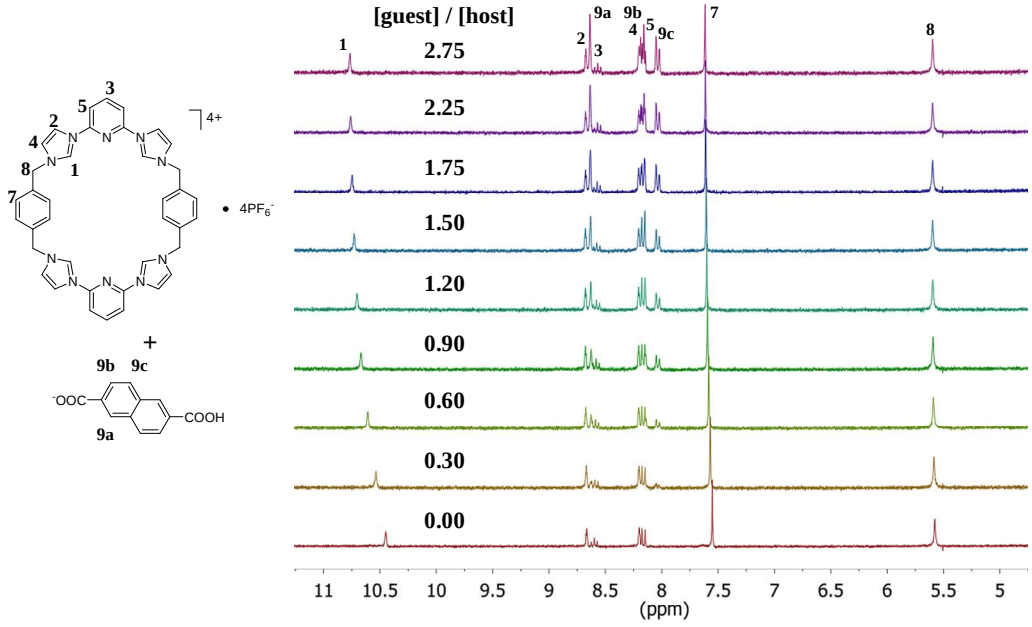

Figure S26. 300 MHz ^{1}H NMR spectroscopic titration of [$\mathbf{1}^{4+}\cdot 4PF_6^-$] ($5.00 \times 10^{-4}$ M) with **9** in DMSO-d_6 at 300 K.

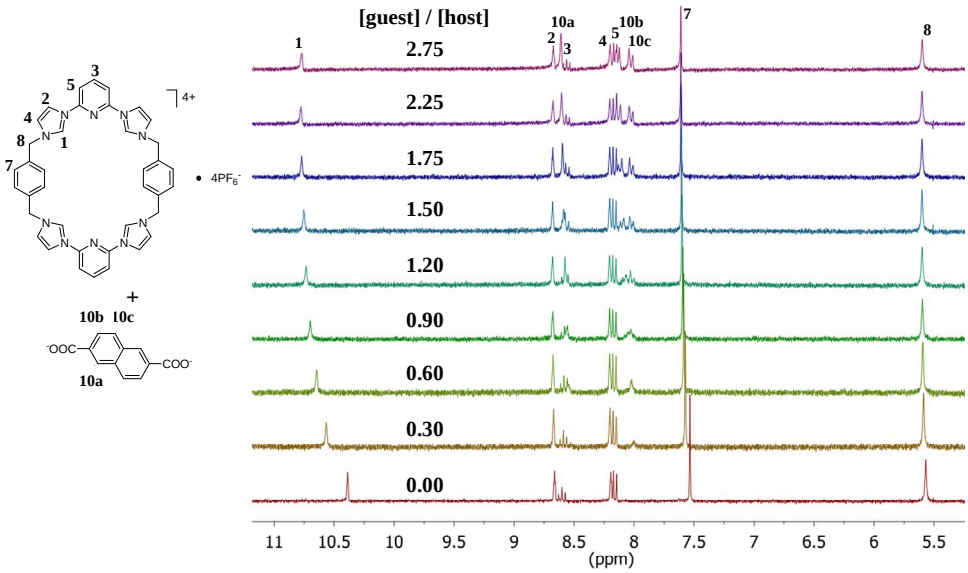

Figure S27. 300 MHz ^{1}H NMR spectroscopic titration of [$\mathbf{1}^{4+}\cdot 4PF_6^-$] ($5.0 \times 10^{-4}$ M) with **10** in DMSO-d_6 at 300 K.

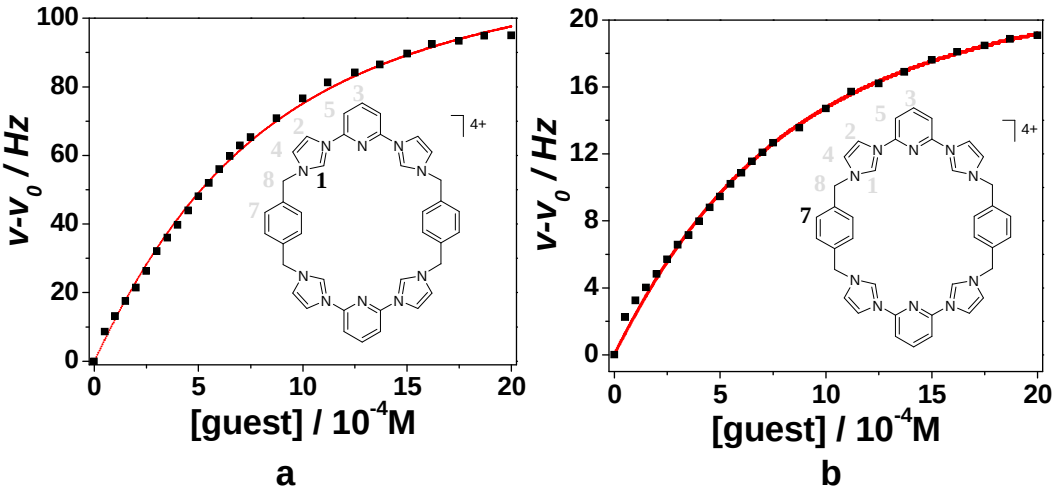

Figure S28. 300 MHz ^{1}H NMR binding isotherms corresponding to the interaction between [$\mathbf{1}^{4+}\cdot 4PF_6^-$] and **9** in DMSO-$d_6$ at 298 K. The chemical shift changes of (**a**) H(1) and (**b**) H(7) on $\mathbf{1}^{4+}$ were used for the calculation of K_1 ($(2.1 \pm 0.1) \times 10^3$ M^{-1}) using the Hyperquad 2003 program. [12] The red dashed lines show the non-linear curve fit of the experimental data to the appropriate equation.

Even though it was not involved in the binding constants calculation, we observed that the signal of H(3) shifts to a higher-field with the addition of **9**. This change provides evidence that π-π donor-acceptor interactions are involved in the formation of pseudorotaxane complex $[\mathbf{1}^{4+}\cdot\mathbf{9}]^{3+}$. Alternatively, the peak corresponding to H(2) slightly shifted to a lower-field and then subsequently shifted back to a higher-field upon the addition of excess guest anion species. This leads us to suggest that excess anion acts π donor to shield the host (*cf.* Figure S29).

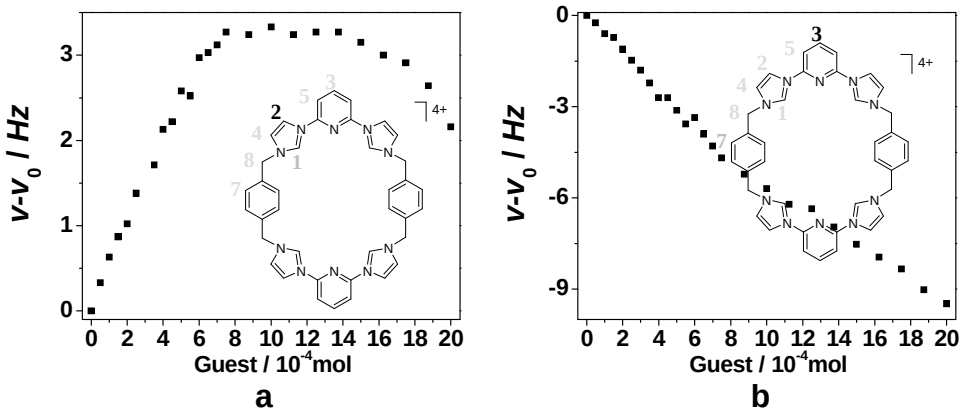

Figure S29. 300 MHz ^{1}H NMR binding isotherms corresponding to the interaction between $[\mathbf{1}^{4+}\cdot 4PF_6^-]$ and **9** in DMSO-d_6 at 298K. The chemical shift changes of (**a**) H(2) and (**b**) H(3) on $\mathbf{1}^{4+}$ were used for the binding mode analysis.

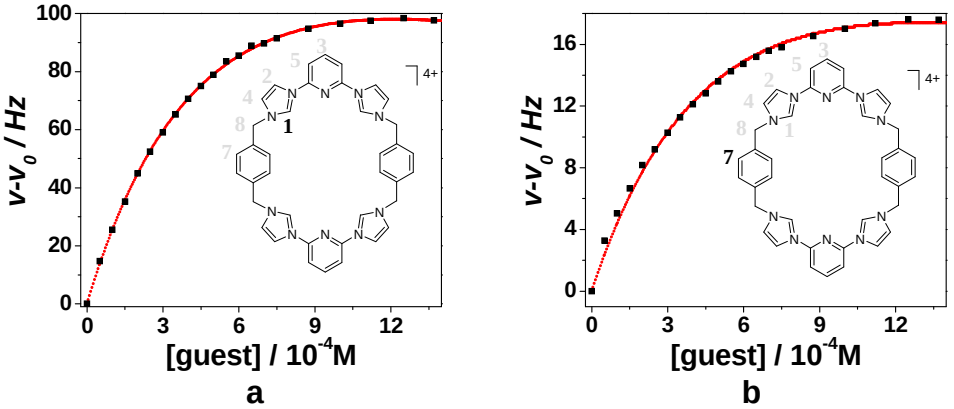

Figure S30. 300 MHz ^{1}H NMR binding isotherms corresponding to the interaction between $[\mathbf{1}^{4+}\cdot 4PF_6^-]$ and **10** in DMSO-d_6 at 298K. The chemical shift changes of (**a**) H(1) and (**b**) H(7) on $\mathbf{1}^{4+}$ were used for the calculation of K_1 ($(3.5 \pm 0.2) \times 10^4$ M^{-1}) using the Hyperquad 2003

program.[12] The red dashed lines show the non-linear curve fit of the experimental data to the appropriate equation.

The signals of H(3) and H(2) show changes in accord with what was previously observed upon the addition of **10.** This leads us to suggest that once again, a pseudorotaxane complex (i.e., $[\mathbf{1}^{4+}\bullet\mathbf{10}]^{2+}$) was generated *via.* 1:1 binding of host and guest through what we believe are $\pi^{\cdots}\pi$ donor-acceptor interactions (*cf.* Figure S31).

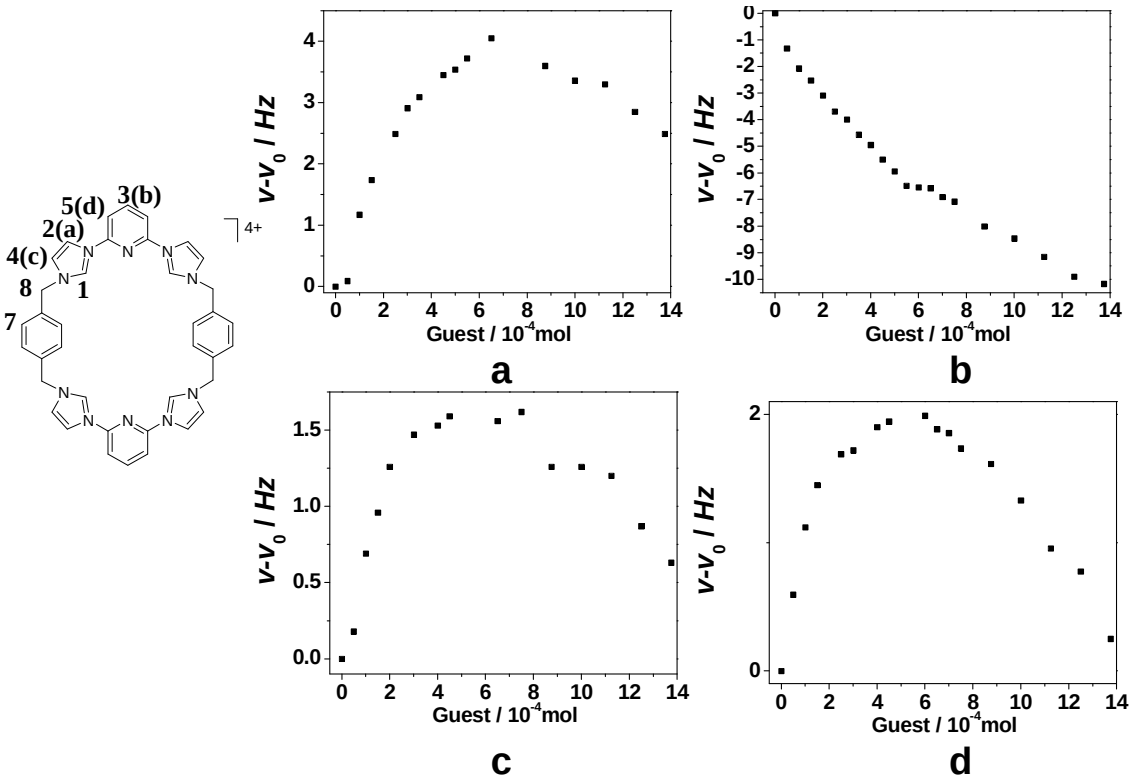

Figure S31. 300 MHz ^{1}H NMR binding isotherms corresponding to the interaction between $[\mathbf{1}^{4+}\cdot 4PF_6^-]$ and **10** in DMSO-d_6 at 298K. The chemical shift changes of (**a**) H(2), (**b**) H(3), (**c**) H(4) and (**d**) H(5) on $\mathbf{1}^{4+}$ were used for the binding mode analysis.

NOESY NMR spectroscopic studies were carried out in an effort to elucidate the nature of the host-guest interactions between macrocycle $\mathbf{1}^{4+}$ and guest anionic species **9** and **10** (Figures S32).[13] Comparative analysis of the resulting spectra for complexes $[\mathbf{1}^{4+}\bullet\mathbf{9}]^{3+}$ and

$[\mathbf{1}^{4+}\cdot\mathbf{10}]^{2+}$ revealed that similar binding modes are involved in pseudorotaxane formation. In both spectra, correlations between H(1) and H(6a, 6b, 6c), H(4) and H(6a), H(7) and H(6a, 6b, 6c), H(8) and H(6a, 6b, 6c) were observed. Additionally, when **10** was analyzed as the guest species there was no overlap signal between the host and guest. Thus, more clean correlations were observed between H(2) and H(6b, 6c), as well as H(5) and H(6a). From these results we suggest that these spectra are consistent with an "insert" binding mode (*i.e.*, the anionic guests are "threaded" through the core of macrocycle $\mathbf{1}^{4+}$ resulting in formation of pseudorotaxane structures).

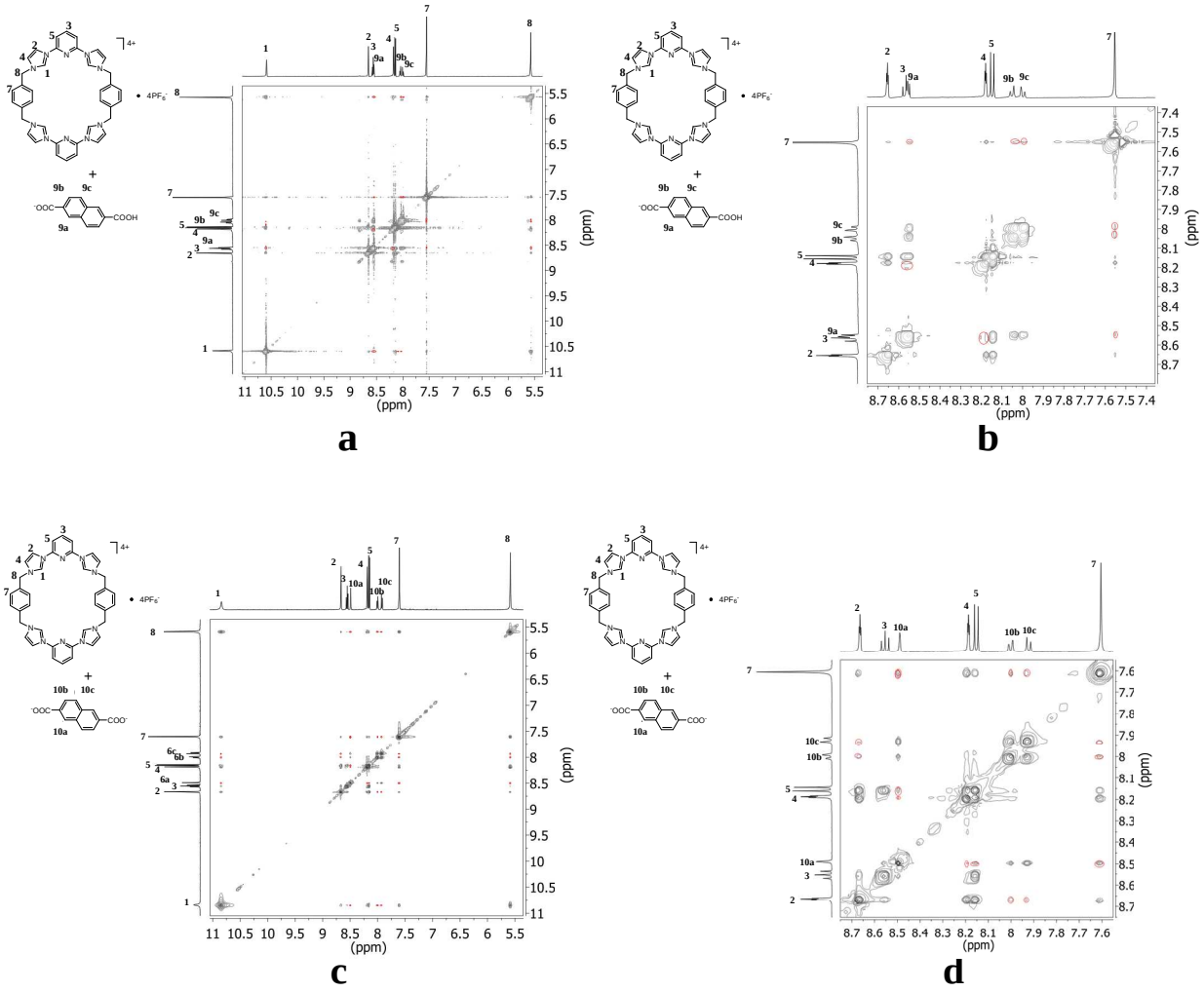

Figure S32. Full views and expansion of the 500 MHz NOESY NMR spectra of $[\mathbf{1}^{4+}\cdot 4PF_6^-]$ (5.00 mM) recorded in the presence of 1 molar equiv of **9** (**a**) and (**b**), and one molar equiv of **10** (**c**) and (**d**) in DMSO-d_6 at 300 K. Correlations were observed as the red highlight signals.

Concentration dependent ^{1}H NMR spectroscopic studies were carried out for pseudorotaxane complex $[\mathbf{1}^{4+}\bullet\mathbf{9}]^{3+}$ (Figure S33).[14]

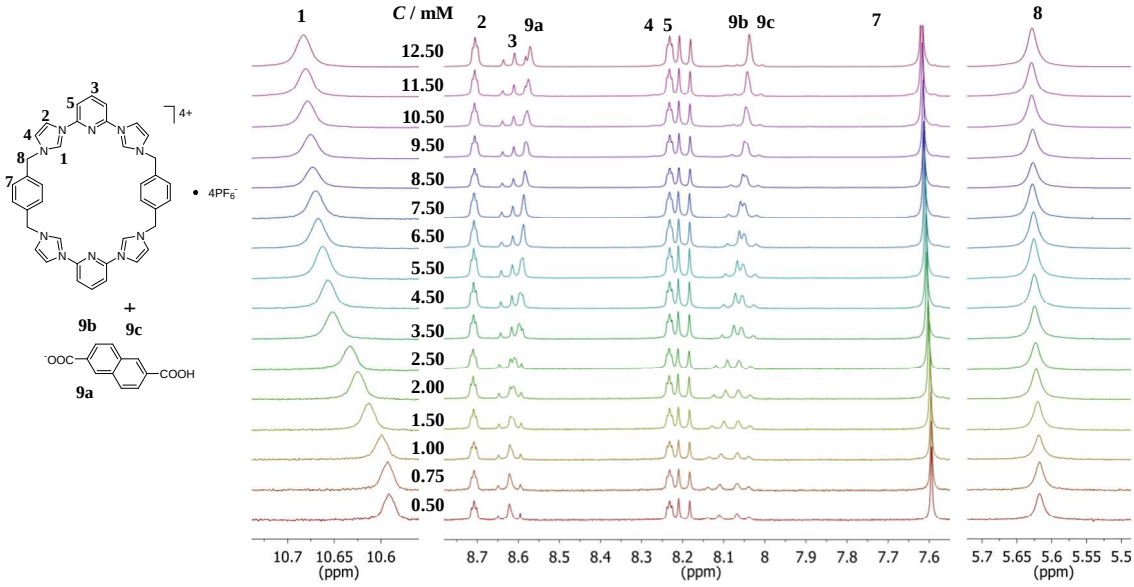

Figure S33. Concentration dependent 300 MHz ^{1}H NMR spectra recorded for $[\mathbf{1}^{4+}\cdot 4PF_6^-]$ in the presence of 1 molar equiv of **9** in DMSO-d_6 at 300 K.

Using the association constants K_1 ($(2.1 \pm 0.1) \times 10^3$ M^{-1}) given in Figure 28, the difference of P_T and P_C at various concentrations was obtained, and from this, the influence of $[\mathbf{1}^{4+}\cdot\mathbf{9}]^{3+}_n$ on the observed chemical shift can be extrapolated (Figure S34). As Figure S34 demonstrates, in the case of pseudorotaxane complex $[\mathbf{1}^{4+}\cdot\mathbf{9}]^{3+}$ P_T and P_C fit well with each other. This leads us to suggest that no linear oligomeric systems are observed in solution.

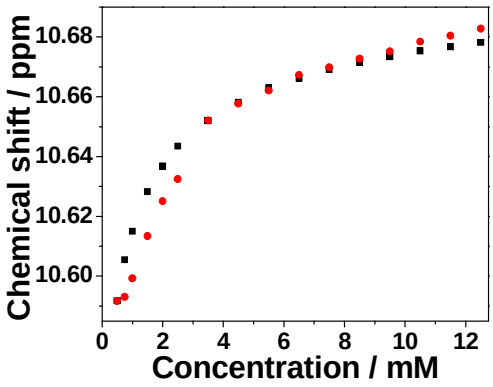

Figure S34. Calculated and observed 300 MHz ^{1}H NMR isotherms for [$\mathbf{1}^{4+}\cdot 4PF_6^-$] and 1 molar equiv **9** in DMSO-d_6 at different concentrations. "■" represents the theoretical NMR shift value P_C of H(1); "●" represents the experimental data P_T of H(1).

Temperature dependent ^{1}H NMR spectroscopic studies were used to obtain further insights into the stability of the resulting pseudorotaxane complexes in solution (Figures S34 and S35). It was observed that the extent of complexation between $\mathbf{1}^{4+}$ and guest anionic species **9** or **10** was reduced upon heating. Pseudorotaxane complexes [$\mathbf{1}^{4+}\cdot\mathbf{9}$]$^{3+}$ and [$\mathbf{1}^{4+}\cdot\mathbf{10}$]$^{2+}$ appear to follow similar trends as the temperature is increased from 300K to 388K. In both species lower-field shifts in the signal associated with H(1) are observed as the temperature is increased (Figures S35 and S36). However, a larger shift was observed in the case of [$\mathbf{1}^{4+}\cdot\mathbf{10}$]$^{2+}$ as compared to [$\mathbf{1}^{4+}\cdot\mathbf{9}$]$^{3+}$ over the previously mentioned temperature range (Figure S36). These spectral changes leads us to propose that similar binding modes are observed for [$\mathbf{1}^{4+}\cdot\mathbf{9}$]$^{3+}$ and [$\mathbf{1}^{4+}\cdot\mathbf{10}$]$^{2+}$, and further support the notion that these complexes are dominated by C-H$^{\cdots}$anion and donor$^{\cdots}$acceptor interactions over the investigated temperature range. Further, we postulate that the stabilization of complex [$\mathbf{1}^{4+}\cdot\mathbf{10}$]$^{2+}$ is influenced to a greater extent, as compared to [$\mathbf{1}^{4+}\cdot\mathbf{9}$]$^{3+}$, by C-H$^{\cdots}$anion interactions.

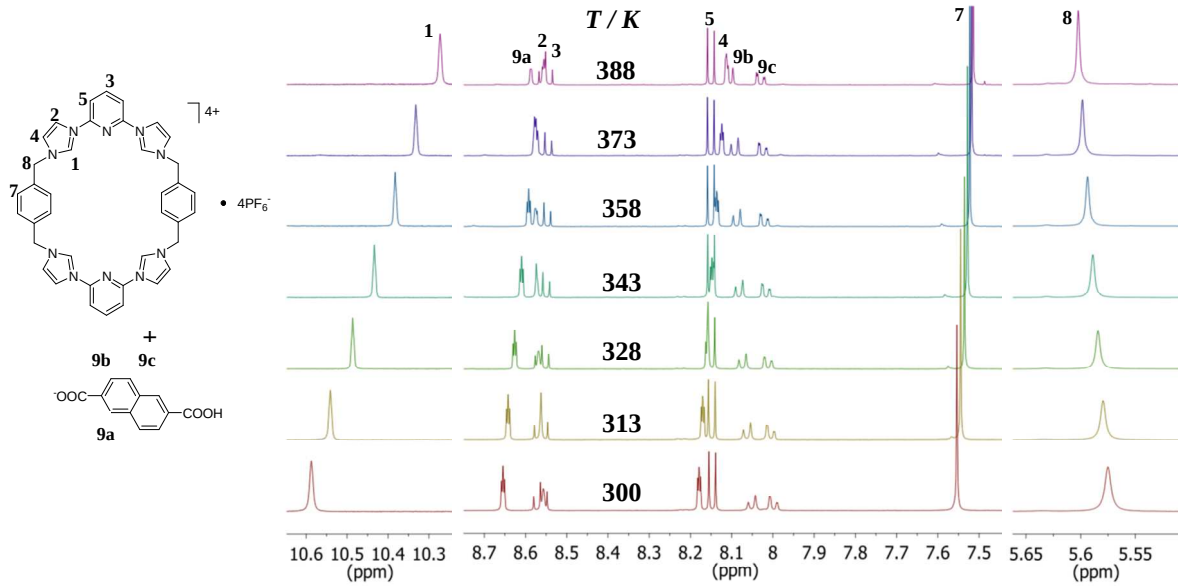

Figure S35. Expansion of the temperature dependent 500 MHz ^{1}H NMR spectra of [$\mathbf{1}^{4+}\cdot 4PF_6^-$] ($5.00 \times 10^{-3}$ M) in the presence of 1 molar equiv **9** in DMSO-d_6 over the 10.6 - 10.1, 8.7 - 7.4, and 5.7 - 5.5 ppm spectral ranges.

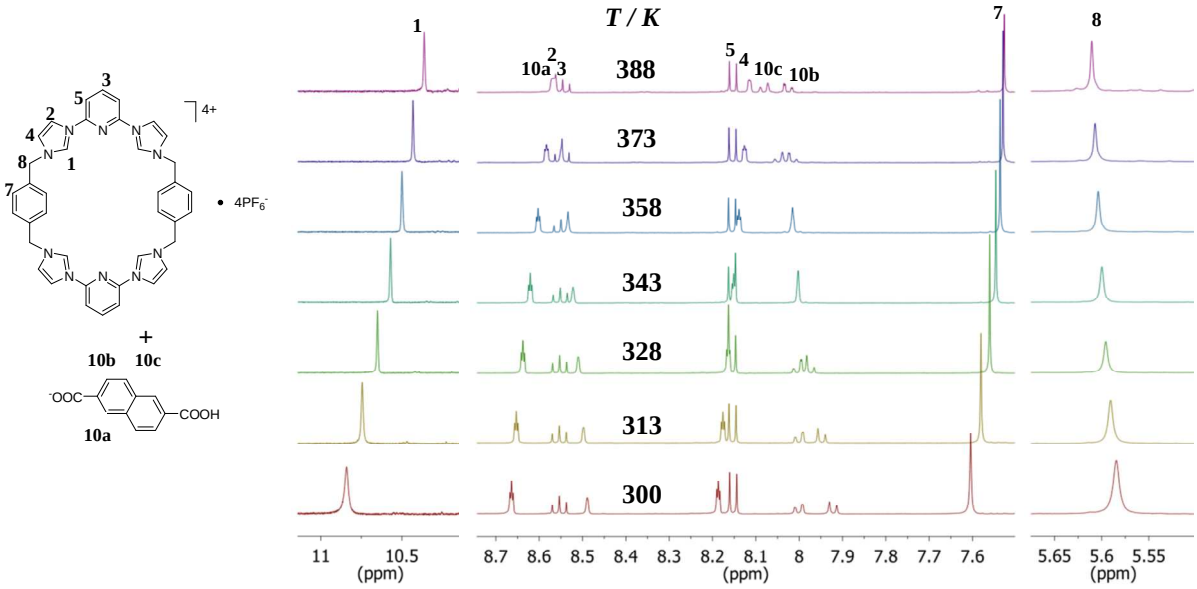

Figure S36. Expansion of the temperature dependent 500 MHz ^{1}H NMR spectra of [$\mathbf{1}^{4+}\cdot 4PF_6^-$] ($5.00 \times 10^{-3}$ M) in the presence of **10** in DMSO-d_6 over the 11.0 - 10.1, 8.7 - 7.4, and 5.7 - 5.5 ppm spectral ranges.

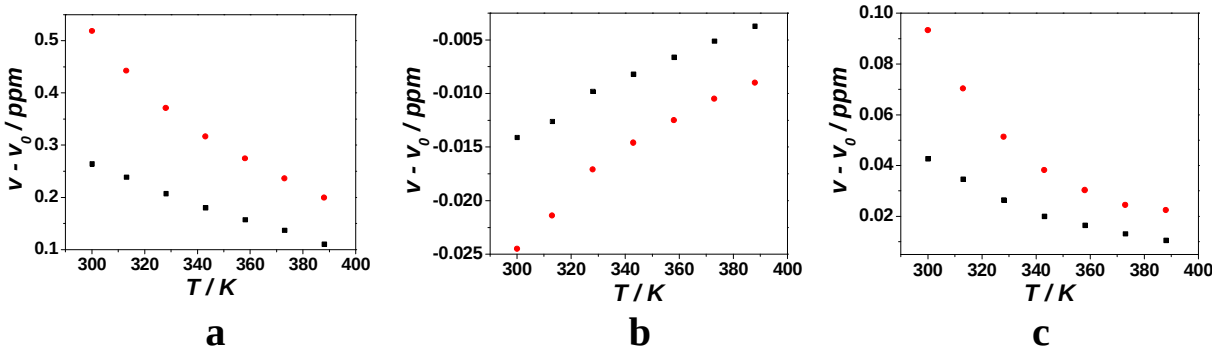

Figure S37. 500 MHz ^{1}H NMR chemical shifts for (**a**) H(1), (**b**) H(3) and (**c**) H(7) of $\mathbf{1}^{4+}\cdot 4PF_6^-$ (5.00 mM) recorded in the presence of 1 molar equiv of varying guest anions in DMSO-d_6 at different temperatures. Here, "■" represents [$\mathbf{1}^{4+}\cdot 4PF_6^-$] in the presence of 1 molar equiv. **9**; "●" represents [$\mathbf{1}^{4+}\cdot 4PF_6^-$] in the presence of 1 molar equiv. **10**.

Next, the effects of pH on pseudorotaxane formation were investigated. Initially, TEA was added to a DMSO-d_6 solution contining $\mathbf{1}^{4+}$ (2.00 mM) and 1 molar equiv of diacid **8.** This resulted in higher-field shift in the signals associated with H(1) and H(7) (Figure S38) leading us to suggest that pseudorotaxane formation was effectively "turned on" by converting the guest species to dianion **10**. Subsequently, the solution was acidified by adding excess deuterium TFA resulted in a lower-field field shift of the signals associated with H(1) and H(7). This leads us to suggest that addition of acid was sufficient in neutralizing dianion **10** effectively converting it back to diacid **8,** which resulted in a dethreading or "turning off" the pseudorotaxane complex. These cycles were repeated as shown in Figure S39. Once again, a dampening of the frequency was observed as the repetitions increased, which is postulated to reflect the strong buffering capabilities of the H(D)TEA$^+$-CF_3COO^- salt that builds up in solution (Figure S40).

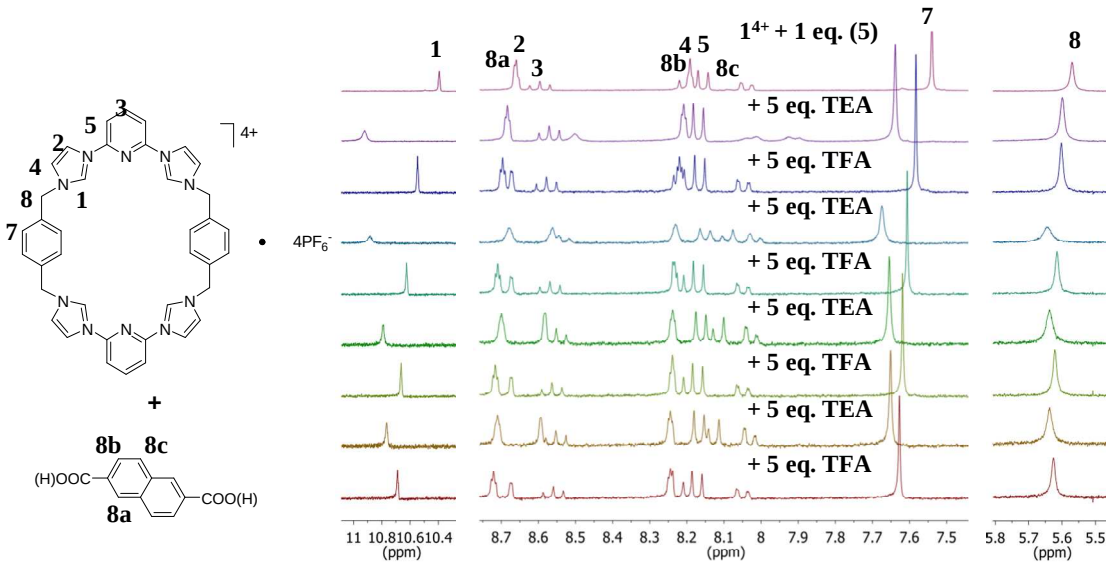

Figure S38. Cycling of the switch as observed by measurement of the 300 MHz ^{1}H NMR spectra at 300 K in DMSO-d_6. The concentration of $\mathbf{1}^{4+}$ has been maintained as 2.00 mM with 1 molar equiv. **8**. The first and later cycles were produced by alternating addition of 5 molar equiv. TEA and 5 molar equiv. CF_3COOD.

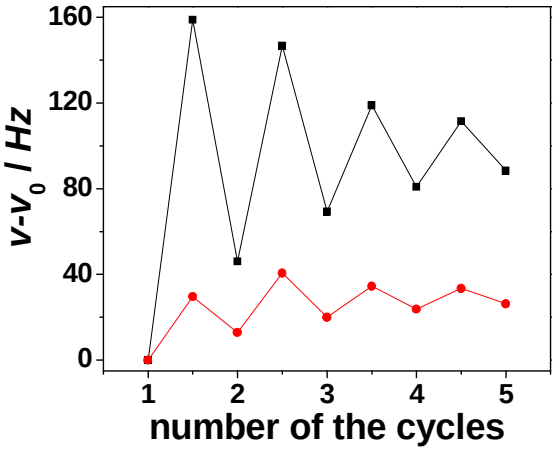

Figure S39. Cycles of pseudorotaxane threading and dethreading as determined by changes in the chemical shift of the 300 MHz ^{1}H NMR signals associated with H(1) (represented as "■") and H(7) (represented as "●") on $\mathbf{1}^{4+}$ at 300 K in DMSO-d_6. The initial concentration of $\mathbf{1}^{4+}$ was maintained throughout the study at 2.00 mM with 1 molar equiv **8**. The first step in each cycle is the addition of 5 molar equiv TEA and the second is the addition of 5 molar equiv CF_3COOD.

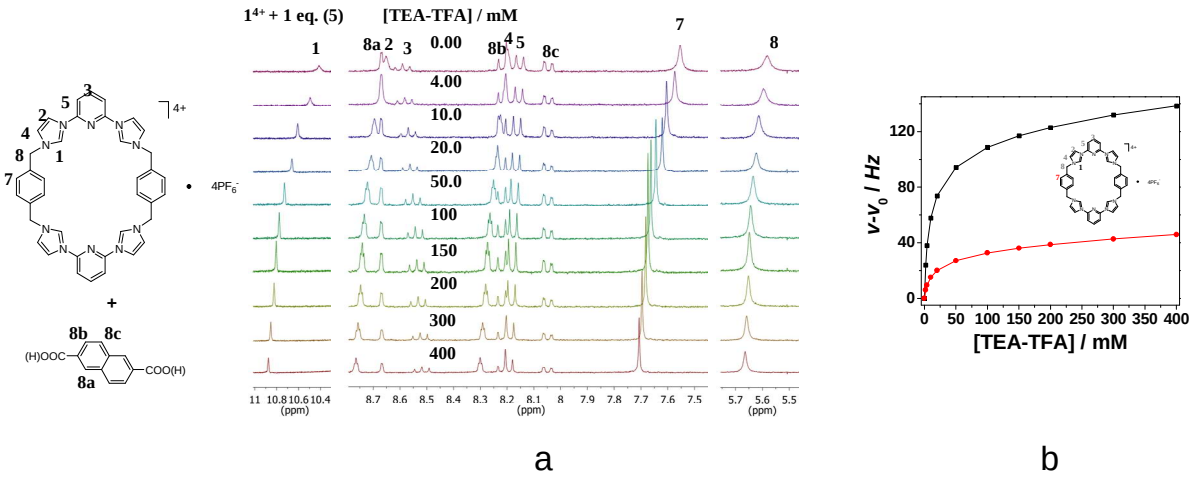

Figure S40. 300 MHz ^{1}H NMR spectroscopic titration of [$\mathbf{1}^{4+}\cdot 4PF_6^-$] ($2.0 \times 10^{-3}$ M) and 1 molar equiv **8** with the addition of H(D)TEA^{+}-CF_3COO^{-} (TEA-TFA) salt in DMSO-d_6 at 300 K as shown by; (a) The ^{1}H NMR spectra and (b) the chemical shift change of H(1) (represented as "■") and H(7) (represented as "●") on $\mathbf{1}^{4+}$ during the titration.

Mass Spectrometric Study

Preliminary results obtained from electrospray mass spectrometry (ESI-MS) experiments that lead us to suggest that at least some of the host/guest interactions may also exist in the gas phase. Analysis of $\mathbf{1}^{4+}$ in the presence of each of the guest moieties **4**, **6**, **7**, **9**, and **10** produced several ions identified as host/guest complexes. The ESI-MS data shown below were acquired via infusion on a Thermo LTQ-XL linear ion trap mass spectrometer operating in positive ion mode.

Table S1. Summary of ESI-MS results. Peak assignments were confirmed by collisional activation (fragmentation) experiments, which produced ions corresponding to the free host in all cases.

Compound	Observed m/z value	Peak Assignment
1 • $\mathbf{4}_2$	265.2	$[\mathbf{1}^{4+} + \mathbf{4} + H]^{3+}$
	397.0	$[\mathbf{1}^{4+} + \mathbf{4}]^{2+}$
1 • $\mathbf{6}_4$	290.8	$[\mathbf{1}^{4+} + \mathbf{6} + H]^{3+\bullet}$
	434.9	$[\mathbf{1}^{4+} + \mathbf{6} - H]^{2+}$
	660.6	$[2\ \bullet\mathbf{1}^{4+} + 3\ \bullet\mathbf{6} - 3H]^{3+\bullet}$
1 • $\mathbf{7}_2$	290.8	$[\mathbf{1}^{4+} + \mathbf{7} + 2H]^{3+\bullet}$
	434.9	$[\mathbf{1}^{4+} + \mathbf{7}]^{2+}$
	660.6	$[2\ \bullet\mathbf{1}^{4+} + 3\ \bullet\mathbf{7}]^{3+\bullet}$
1 • $\mathbf{9}_4$	281.8	$[\mathbf{1}^{4+} + \mathbf{9} - 2H]^{3+\bullet}$
	421.8	$[\mathbf{1}^{4+} + \mathbf{9} - H]^{2+}$
1 • $\mathbf{10}_2$	281.8	$[\mathbf{1}^{4+} + \mathbf{10} + H]^{3+\bullet}$
	421.8	$[\mathbf{1}^{4+} + \mathbf{10}]^{2+}$

Additionally, the mass spectrometric study also showed that multi-component oligomeric species derived from $\mathbf{1}^{4+}$, **10** and Ag(I) also survived in the gas phase. Here the ESI-MS data was acquired by infusing solution of [$\mathbf{1}^{+4}$• (**10**)$_3$• Ag_2• 16 H_2O] in DMF/acetonitrile/water (1:1:1, v/v/v) into a Thermo LTQ-XL linear ion trap mass spectrometer operating in positive ion mode. UltraZoomScan and MS^n experiments were performed as necessary to confirm charge state and formula assignments.

Table S2. Summary of ESI-MS Results of [$\mathbf{1}^{4+}$• (**10**)$_3$• Ag_2• 16 H_2O].

Ion (m/z)	Assignment
314.3	$(\mathbf{1}^{4+} - 2H)^{+2}$
421.2	$(\mathbf{1}^{4+} - 4H + 2\ Ag)^{+2}$
627.3	$(\mathbf{1}^{4+} - 3H)^{+}$
733.2/735.2[a]	$(\mathbf{1}^{4+} - 4H + Ag)^{+}$; $(2\ \bullet\mathbf{1}^{4+} - 4H + \mathbf{10})^{+2}$
841.1/843.1[a]	$(\mathbf{1}^{4+} - 5H + 2Ag)^{+}$; $(\mathbf{1}^{4+} - 3H + \mathbf{10})^{+}$
949.1	$(2\ \bullet\mathbf{1}^{4+} - 6H + \mathbf{10} + 4\ Ag)^{+2}$
1057.0[b]	$(2\ \bullet\mathbf{1}^{4+} - 6H + 2\ \bullet\mathbf{10} + 4\ Ag)^{+2}$; $(\mathbf{1}^{4+} - 5H + \mathbf{10} + 2\ Ag)^{+}$
1156.7	$(3\bullet\mathbf{1}^{4+} - 6H + 2\ \bullet\mathbf{10})^{+2}$

[a]Assignments supported by UltraZoomScan experiments
[b]Assignments supported by UltraZoomScan and MS^n experiments

Single Crystal X-ray Analyses

Table S3. X-ray crystallographic data summary of [$\mathbf{1}^{4+}\cdot(\mathbf{4})_2\cdot 16\ H_2O$], [$\mathbf{1}^{4+}\cdot(\mathbf{7})_2\cdot 2$ DMF $\cdot 7.5\ H_2O$], **[**$\mathbf{1}^{4+}\cdot(\mathbf{10})_2\cdot 10\ H_2O$], and [$\mathbf{1}^{4+}\cdot(\mathbf{10})_3\cdot Ag_2\cdot 16\ H_2O$].

	$\mathbf{1}^{4+}\cdot(\mathbf{4})_2\cdot 16\ H_2O$	$\mathbf{1}^{4+}\cdot(\mathbf{7})_2\cdot 2$ DMF $\cdot 7.5\ H_2O$	$\mathbf{1}^{4+}\cdot(\mathbf{10})_2\cdot 10\ H_2O$	$\mathbf{1}^{4+}\cdot(\mathbf{10})_3\cdot Ag_2\cdot 16\ H_2O$
CCDC No.	775822	775824	775820	784454
description	plate	block	block	plate
color	colorless	colorless	light yellow	colorless
From solution	Water/ acetonitrile	Water/ acetonitrile /DMF	Water/ acetonitrile /DMF	Water/ acetonitrile /DMF
empirical formul	$C_{54}H_{42}N_{10}O_{24}$	$C_{72}H_{64}N_{12}O_{17.5}$	$C_{62}H_{66}N_{10}O_{18}$	$C_{74}H_{52}Ag_2N_{10}O_{28}$
Mr	1214.98	1377.35	1239.25	1745.00
crystal size (mm^3)	0.27 × 0.18 × 0.06	0.31 × 0.26 × 0.23	0.43 × 0.15 × 0.08	0.30 × 0.15 × 0.09
crystal system	Triclinic	Triclinic	Triclinic	Triclinic
space group	P-1	P-1	P-1	P-1
a [Å]	10.421(2)	10.807(2)	11.018(2)	11.431(2)
b [Å]	11.556(2)	12.716(3)	12.439(3)	13.858(3)
c [Å]	14.011(3)	14.113(3)	12.576(3)	15.183(3)
α [deg]	98.76(3)	69.89(3)	118.73(3)	116.200(3)
β [deg]	109.73(3)	82.26(3)	99.56(3)	91.130(3)
γ[deg]	101.49(3)	72.19(3)	91.47(3)	113.540(3)
V/ [$Å^3$]	1511.5(5)	1733.0(6)	1479.3(5)	1921.4(7)
d/[g/cm^3]	1.335	1.320	1.391	1.508
Z	1	1	1	1

T [K]	223(2)	223(2)	173(2)	173(2)
R1, wR2 I > 2ó(I)	0.1062, 0.2257	0.0800, 0.2008	0.0766, 0.1924	0.0925, 0.1909
R1, wR2 (all data)	0.1687, 0.2814	0.0872, 0.2068	0.0864, 0.2016	0.1240, 0.2209
quality of fit	0.966	0.871	1.012	0.978

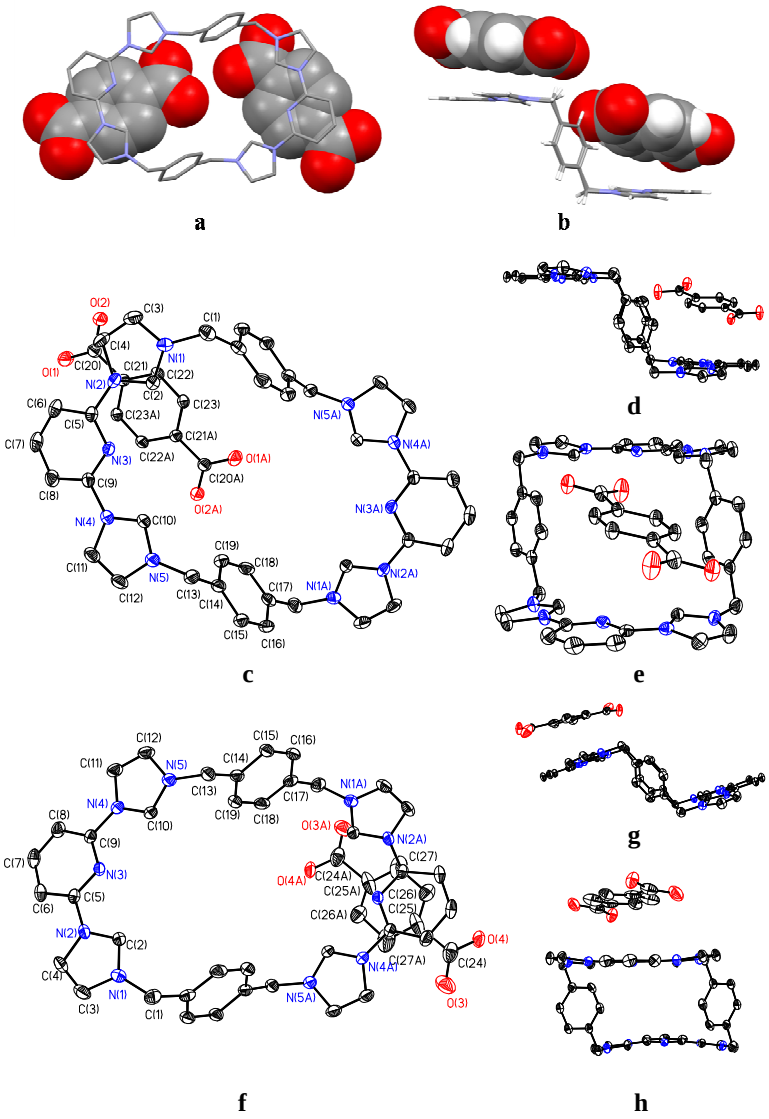

Figure S41. Single X-ray crystal structure of [$\mathbf{1}^{4+}\cdot(\mathbf{4})_2\cdot 16\ H_2O$]. All solvent molecules have been omitted for clarity. Top view (a) and side view (b) of the interaction between $\mathbf{1}^{4+}$ and the

two molecules of **4**. Top view (c) and side views (d) and (e) of the first of two 'outer' binding modes in the structure of [$\mathbf{1}^{4+}\cdot(\mathbf{4})_2\cdot 16\ H_2O$]. Possible $\pi\cdots\pi$ donor-acceptor interactions are revealed in the following selected interatomic distances [Å]: C(21)···N(2) 3.693, C(22)···N(2) 3.446, C(23)···C(2) 3.664, C(23A)···C(6) 3.730. Top view (f), and side view (g) and (h) of the second 'outer' binding mode seen in the structure of [$1^{4+}\cdot(2)_2\cdot 16\ H_2O$]. Possible anion$\cdots\pi$ interaction as revealed by selected interatomic distances [Å]: C(24)···C(7A) 3.634, C(24)···C(8A) 3.494, C(25)···C(9A) 3.506, C(26)···C(5A) 3.402, C(27)···N(2A) 3.241, C(24A)···C(2A) 3.473, C(27A)···N(4A) 3.527, O(3)···C(8A) 3.418, O(3A)···N(1A) 3.483. The results from the two methods of analysis (NMR spectroscopy and X-ray diffraction) are in good agreement with 'outside' binding modes.[14]

Analysis of the single crystal X-ray structure of complex [$\mathbf{1}^{4+}\cdot(\mathbf{7})_2\cdot 2DMF\cdot 7.5H_2O$] revealed the formation of a pseudorotaxane structure stabilized through multiple intermolecular anion$\cdots\pi$ interactions (*cf.* Figure S42). Two neighboring pseudorotaxane units are bound to each other through one subunit of **7** through what is presumed to be strong $\pi\cdots\pi$ donor$\cdots$acceptor interactions (*cf.* Figure 43). Again, a 1D self assembled system with apparent donor-acceptor-donor (DAD) interactions was observed (*cf.* Figure S44).

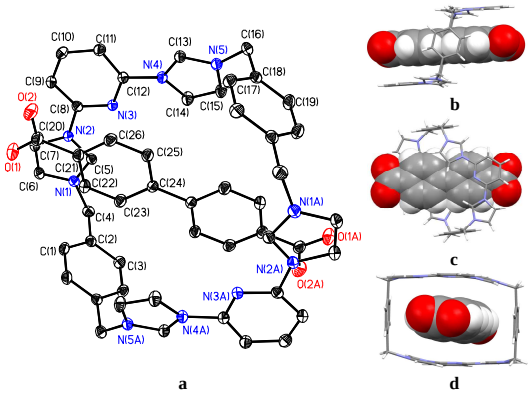

Figure S42. Single crystal X-ray structure of the pseudorotaxane structure [$\mathbf{1}^{4+}\cdot(\mathbf{7})_2\cdot$2 DMF$\cdot$7.5 H_2O] from; (a) the view of the pseudorotaxane complex [$\mathbf{1}^{4+}\cdot\mathbf{7}]^{2+}$ present in [$\mathbf{1}^{4+}\cdot(\mathbf{7})_2\cdot$2 DMF$\cdot$7.5 H_2O] showing the atom labeling scheme as well as top (b) and side views (c) and (d) of the pseudorotaxane structure. Displacement ellipsoids are scaled to the 25% probability level. The entire assembly sits around a crystallographic inversion center at ½, ½, ½. Selected interatomic distances [Å]: O(1)···C(7) 3.608, O(1)···N(2) 3.698, O(1)···C(8) 3.608, O(1)···C(9) 3.394, O(2)···C(9) 3.702, O(2)···C(10) 3.545, C(20)···C(8) 3.552, C(20)···C(9) 3.365, C(20)···C(10) 3.648, C(21)···C(8) 3.472, C(21)···C(9) 3.760, C(21)···C(12) 3.701, C(21)···N(3) 3.425, C(22)···C(5) 3.543, C(22)···N(2) 3.475, C(22)···C(8) 3.568, C(22)···N(3) 3.583, C(25)···C(13) 3.774, C(25)···N(4) 3.457, C(25)···C(14) 3.681, C(26)···C(11) 3.750, C(26)···C(12) 3.365, C(26)···N(3) 3.502, C(26)···N(4) 3.633.

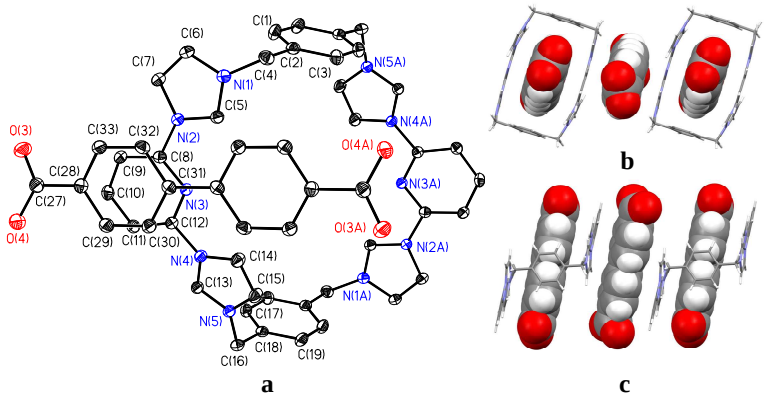

Figure S43. Extended single crystal packing structure showing formation of a 1D 'DAD' self-assembly complex. This figure shows one set of views designed to highlight the interaction between two neighboring pseudorotaxane "monomer" units present in the complex [$\mathbf{1}^{4+}\cdot(\mathbf{7})_2\cdot$2 DMF$\cdot$7.5 H_2O] from; (a) a view showing the atom labeling scheme of the complex containing only a molecule of **7** bound the outer periphery (the inserted molecule of **7** has been removed for clarity), as well as side views (b) and (c) of two neighboring pseudorotaxane units with a bridging molecule of **7**. From this structure it is presumed that the stabilizing interactions between these two units are predominantly anion$\cdots\pi$ interactions as determined using the selected interatomic distances [Å]: O(3)$\cdots$C(9) 3.514, C(27)$\cdots$C(9) 3.530, C(27)$\cdots$C(10) 3.621, C(28)$\cdots$C(8) 3.538, C(28)$\cdots$C(9) 3.333, C(28)$\cdots$C(10) 3.701, C(29)$\cdots$N(3) 3.671, C(29)$\cdots$C(8) 3.659, C(29)$\cdots$C(9) 3.727, C(29)$\cdots$C(10) 3.801, C(29)$\cdots$C(11) 3.800, C(29)$\cdots$C(12) 3.711, C(30)$\cdots$C(8) 3.724, C(30)$\cdots$C(12) 3.737, C(30)$\cdots$N(3) 3.447, C(29)$\cdots$C(8) 3.659, C(31)$\cdots$N(3) 3.655, C(31)$\cdots$C(8) 3.730, C(31)$\cdots$N(2) 3.676, C(31)$\cdots$C(5) 3.585, C(32)$\cdots$C(5) 3.469, C(32)$\cdots$C(7) 3.655, C(32)$\cdots$C(8) 3.628, C(32)$\cdots$N(2) 3.300, C(33)$\cdots$C(7) 3.626, C(33)$\cdots$C(8) 3.506, C(33)$\cdots$C(9) 3.586, C(33)$\cdots$N(2) 3.482.

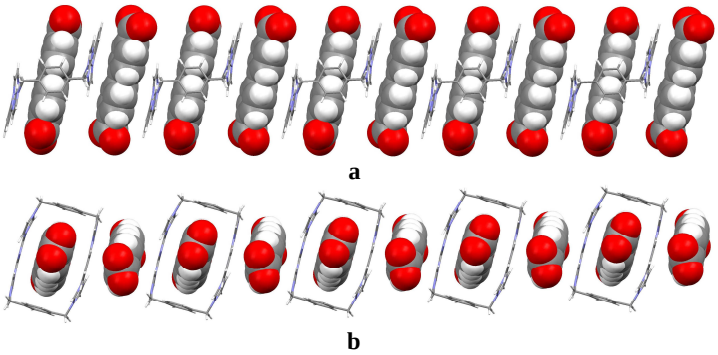

Figure S44. The 1D 'DAD' structure, $[(\mathbf{1}^{4+}\bullet(\mathbf{7}))^{2+}\bullet(\mathbf{7})]_n$, built up from individual pseudorotaxane subunits.

As determined from the single crystal X-ray structure of $[\mathbf{1}^{4+}\cdot(\mathbf{10})_2\cdot 10\ H_2O]$, one molecule of **10** is inserted into the cavity of $\mathbf{1}^{4+}$ to form a pseudorotaxane complex (*cf.* Figure S45). Additionally a second molecule of **10** acts as bridge linking two different pseudorotaxane units by hydrogen bonding (*cf.* Figure S46). As highlighted by Figure S47, a 1D self-assembled complex is built up from individual pseudorotaxane units, a bridging molecule of **10**, and water molecules.

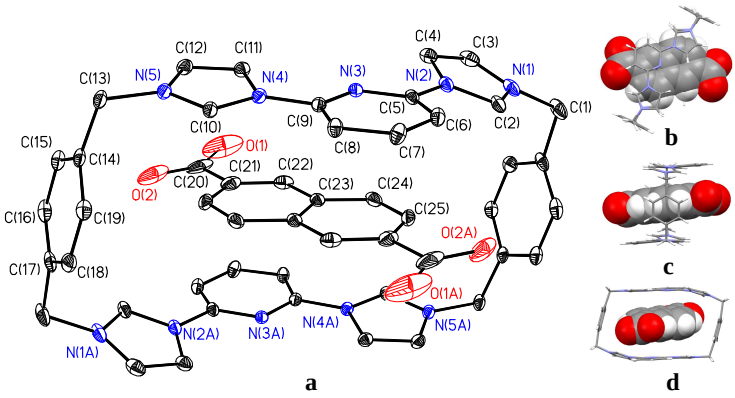

Figure S45. The pseudorotaxane complex $[\mathbf{1}^{4+}\cdot(\mathbf{10})_2\cdot 10\ H_2O]$ as determined from the single crystal X-ray structure, shown from; (a) the atom-labeling scheme of the pseudorotaxane complex, as well as the Top (b) and side views (c) and (d) of the pseudorotaxane structure.

Displacement ellipsoids are scaled to the 25% probability level. The entire assembly sits around a crystallographic inversion center at ½, ½, ½. Selected interatomic distances [Å]: O(1)···C(7) 3.441, O(2)···C(6) 3.296, O(2)···C(7) 3.726, C(20)···C(6) 3.300, C(20)···C(7) 3.344, C(21)···C(5) 3.400, C(21)···N(3) 3.580, C(21)···C(9) 3.729, C(22)···C(8) 3.475, C(22)···C(9) 3.336, C(22)···N(3) 3.556, C(23)···N(3) 3.606, C(23)···C(9) 3.501, C(23)···N(4) 3.510, C(24)···C(10) 3.552, C(24)···N(4) 3.413, C(24)···C(11) 3.647, C(25)···C(11) 3.669, C(25)···C(12) 3.638.

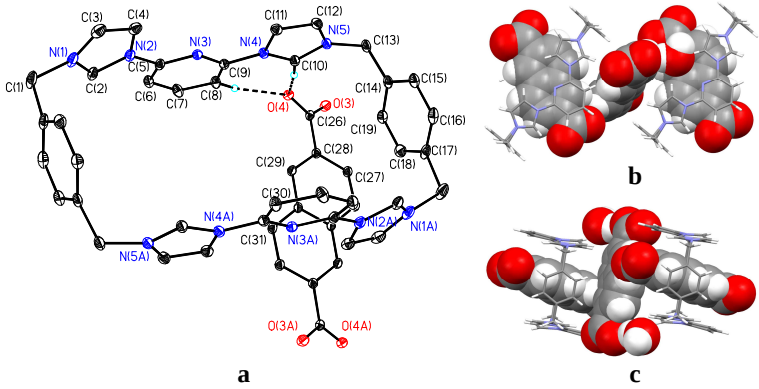

Figure S46. Extended single crystal packing structure showing formation of the 1D self-assembled system in the structure of $[\mathbf{1}^{4+}\cdot(\mathbf{10})_2\cdot 10\ H_2O]$ as shown from; (a) the atom-labeling scheme of the pseudorotaxane complex, as well as the Top (b) and side views (c) and (d) of the pseudorotaxane structure. This extended structure is presume to be stabilized by hydrogen bonding interactions as determined from the selected interatomic distances [Å]: C(8)···O(4) 3.336, C(10)···O(4) 3.013. Selected bond angles C(8)-H(8A)···O(4) 169.16º, C(10)-H(10A)···O(4) 168.34º and 2) also provide evidence for CH···π interactions for which a selected interatomic distance [Å] is C(19)···C(28) 3.695.

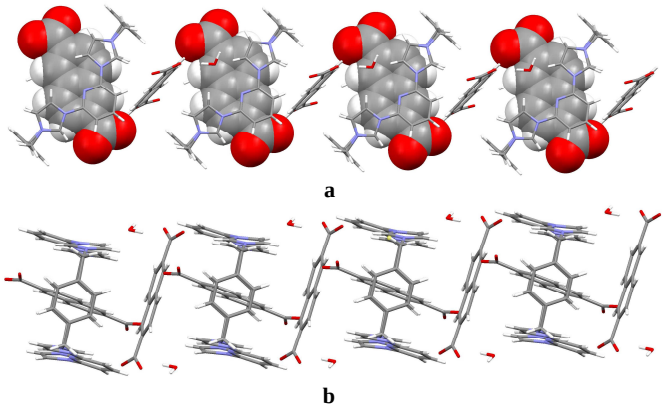

Figure S47. Views of the 1D extended structure show pseudorotaxane assembly into $[(\mathbf{1}^{4+}\cdot(\mathbf{10}))^{2+}\cdot(\mathbf{10})]_n$.

Separately, single crystal structural analysis revealed formation of an extended metal-linked polyrotaxane structure in which the subunits have the formal stoichiometry $[\mathbf{1}^{4+}\cdot(\mathbf{10})_3\cdot Ag_2\cdot 16\ H_2O]$ (Figure S48A and B). Here, dianionic subunits $[(\mathbf{10})_2\cdot Ag_2]^{2-}$, combine with one molecule of **10** interpenetrated into $\mathbf{1}^{4+}$, to create an extended metal-linked complex in the form of a polyrotaxane (Figure S48c). The resulting molecular chains are stacked within the crystal lattice to form a highly ordered arrangement as shown in Figure S48d stabilized, presumably, *via* vertical 'DAD' donor-acceptor interactions between subunits present on neighbor chains.

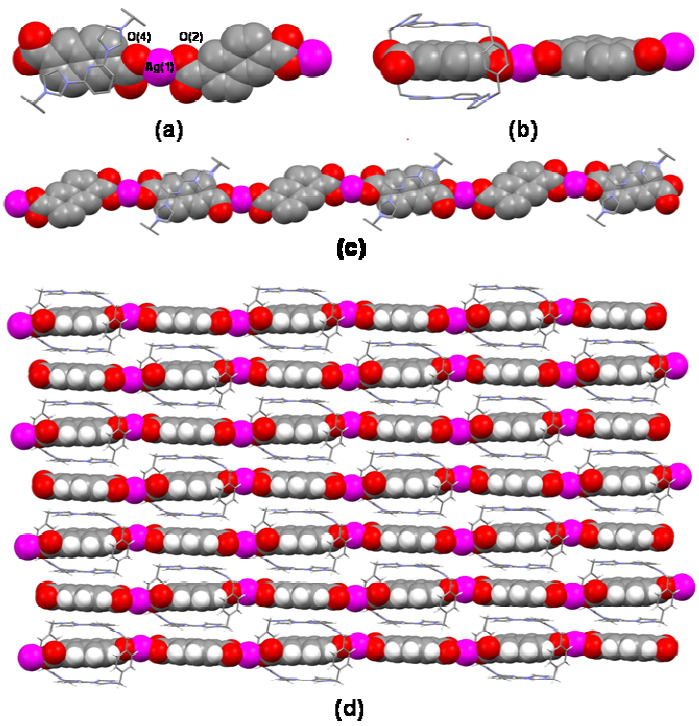

Figure S48. View of the single crystal structure of [$\mathbf{1}^{4+}\cdot(\mathbf{10})_3\cdot Ag_2\cdot 16\ H_2O$] from the top (a) and side (b) views of the pseudorotaxane subunit of [$\mathbf{1}^{4+}\cdot(\mathbf{10})_2\cdot Ag_2]^{2+}$, as well as the top view (c) of the polyrotaxane chain consisting of [$\mathbf{1}^{4+}\cdot(\mathbf{10})_2\cdot Ag_2]_n^{2n+}$. Also a side view (d) of the ordered 2D array comprised of polyrotaxane chains is shown.

Comparison of Pseudorotaxane Complexes

A comparison of the interactions between [$\mathbf{1}^{4+}\cdot 4PF_6^-$] and guest molecules **2** - **10** are shown and provide a better understanding of the receptor properties of macrocycle $\mathbf{1}^{4+}$ as molecular building block.[16]

Table S4. A brief summary showing the nature of the complexes formed in solution from $\mathbf{1}^{4+}\cdot 4PF_6^-$ and guest species **3**, **4**, **6**, **7**, **9**, and **10**.

Guest	Pseudorotaxane structure formation
mono-terephthalate anion (**3**)	*Yes*
di-terephthalate anion (**4**)	*No*
mono-4,4'-biphenyldicarboxylate anion (**6**)	*Yes*
di-4,4'-biphenyldicarboxylate anion (**7**)	*Yes*
mono-2,6-naphthalenedicarboxylate anion (**9**)	*Yes*
di-2,6-naphthalenedicarboxylate anion (**10**)	*Yes*

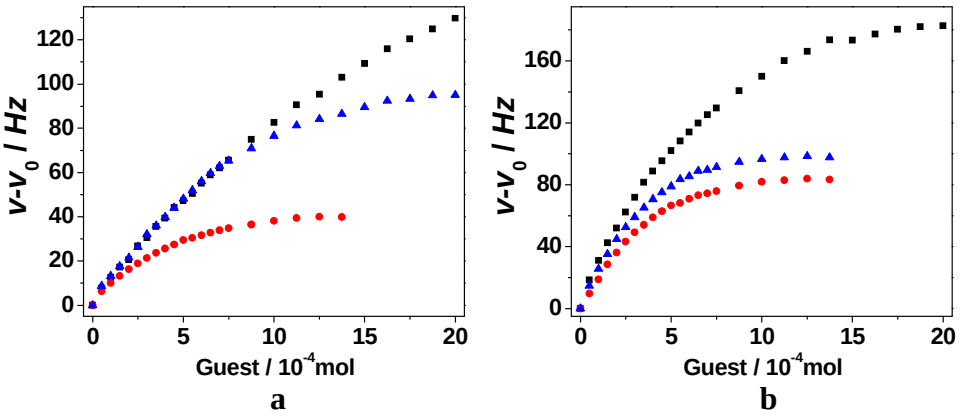

Figure S49. Comparison of 300 MHz ^{1}H NMR binding isotherms of H^1 on $\mathbf{1}^{4+}$ corresponding to the interaction between [$\mathbf{1}^{4+}\cdot 4PF_6^-$] and (a) mono-anion guests **3** (■) , **6** (●), and **9** (▲), as well as (b) dianion guests **4** (■), **7** (●), and **10** (▲) in DMSO-d_6 at 298 K. During the

titration the concentration of the host was maintained at 0.5 mM. The chemical shift changes associated with the signal of H(1) on $\mathbf{1}^{4+}$ were used for the comparison.

Table S4. Summary of the calculated association constants K_a for the complexes formed between $\mathbf{1}^{4+}\cdot 4PF_6^-$ and the mono- and di-terephthalate, 4,4'-biphenyldicarboxylate, and 2,6-naphthalenedicarboxylate anions.

Guest	Equilibrium	Association constants K_a
mono-terephthalate anion	$\mathbf{[H] + [G] \overset{K_1}{\rightleftharpoons} [H\cdot G]}$ $\mathbf{2[H\cdot G] + [G] \overset{K_2}{\rightleftharpoons} [H_2\cdot G_3]}$	$K_1 = (2.1 \pm 0.1) \times 10^3\ M^{-1}$ $K_2 = (2.4 \pm 0.2) \times 10^5\ M^{-2}$
di-terephthalate anion	$\mathbf{[H] + [G] \overset{K_1}{\rightleftharpoons} [H\cdot G]}$	$K_1 = (3.3 \pm 0.1) \times 10^3\ M^{-1}$
mono-4,4'-biphenyldicarboxylate anion	$\mathbf{[H] + [G] \overset{K_1}{\rightleftharpoons} [H\cdot G]}$ $\mathbf{2[H\cdot G] + [G] \overset{K_2}{\rightleftharpoons} [H_2\cdot G_3]}$	$K_1 = (1.5 \pm 0.1) \times 10^3\ M^{-1}$ $K_2 = (1.8 \pm 0.2) \times 10^7\ M^{-2}$
di-4,4'-biphenyldicarboxylate anion	$\mathbf{[H] + [G] \overset{K_1}{\rightleftharpoons} [H\cdot G]}$ $\mathbf{2[H\cdot G] + [G] \overset{K_2}{\rightleftharpoons} [H_2\cdot G_3]}$	$K_1 = (1.8 \pm 0.2) \times 10^3\ M^{-1}$ $K_2 = (1.1 \pm 0.1) \times 10^7\ M^{-2}$
mono-2,6-naphthalenedicarboxylate anion	$\mathbf{[H] + [G] \overset{K_1}{\rightleftharpoons} [H\cdot G]}$	$K_1 = (2.1 \pm 0.1) \times 10^3\ M^{-1}$
di-2,6-naphthalenedicarboxylate anion	$\mathbf{[H] + [G] \overset{K_1}{\rightleftharpoons} [H\cdot G]}$	$K_1 = (3.5 \pm 0.2) \times 10^4\ M^{-1}$

Comparative analysis was carried out using the concentration dependant ^{1}H NMR studies (described above) of pseudorotaxane complexes formed from $\mathbf{1}^{4+}$ and mono-anionic guest species. Here, only guest **3** showed large differences between P_C and P_T, as well as a lower-field shift in the signal associated with H(1) on $\mathbf{1}^{4+}$ as the overall solution concentration was increased. These results provide support for the notion that the existence of high-order

oligomer is only seen in the case of mono-anionic species **3**. This is in good agreement with the results obtained from NOESY NMR and mass spectroscopic analysis. In contrast, in the case of complexes formed from $\mathbf{1}^{4+}$ and guest species **6** and **9**, the value of P_C and P_T fit well with each other leads us to suggest that there are no oligomeric species formed in higher concentration solutions.

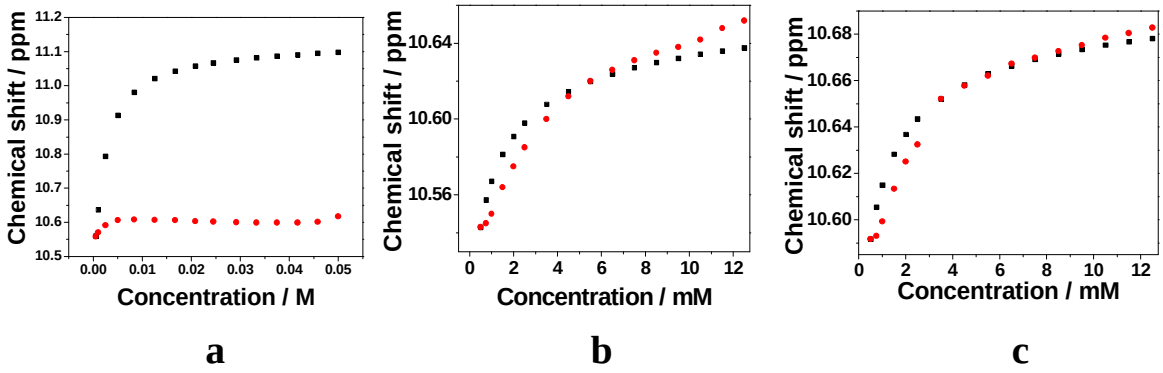

Figure S50. Calculated shift (P_T (■)) and observed shift (P_C (●)), as determined by the chemical shifts associated with H(1) in the 300 MHz ^{1}H NMR isotherms of [$\mathbf{1}^{4+}\cdot 4PF_6^-$] in the presence of 1 molar equiv of guests **3** (a)**, 6** (b), and **9** (c) in DMSO-d_6 as the overall solution concentration was increased.

The single crystal X-ray structures of pseudorotaxane complexes [$\mathbf{1}^{4+}$•**3**•$3PF_6^-$•$4H_2O$], [$\mathbf{1}^{4+}$•**7**•$7.5H_2O$], and [$\mathbf{1}^{4+}$•**10**•$10\ H_2O$] were analyzed by comparative analysis (Figures S51 and S52). The aforementioned structures provide evidence for the dynamic nature of receptor $\mathbf{1}^{4+}$, as it is able to alter the shape and size if its cavity to accommodate different guest species. The structures shown below adapt a variety of different structural conformation as seen here in the form of a 'part chair' conformation for [$\mathbf{1}^{4+}$•**3**]$^{3+}$ (Figure 52 a-d), a 'complete chair II' conformation for [$\mathbf{1}^{4+}$•**7**]$^{2+}$ (Figure 52 e-h), and the 'regular box' conformation for [$\mathbf{1}^{4+}$•**10**]$^{2+}$ (Figure 52 i-l).

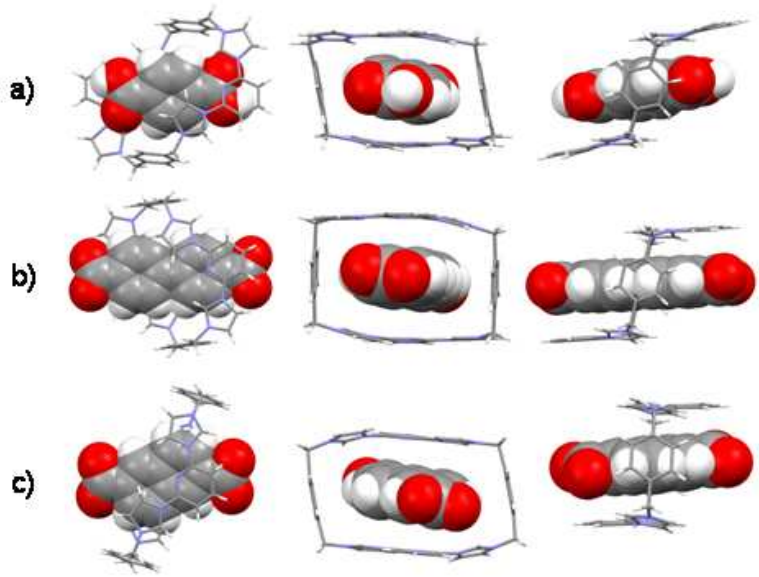

Figure 51. Single X-ray crystal structures of the three pseudorotaxane complexes formed using molecular receptor $\mathbf{1}^{4+}$ and anionic guest species **3**, **7**, and **10**. Some and/or all of the solvent molecules have been omitted for clarity.

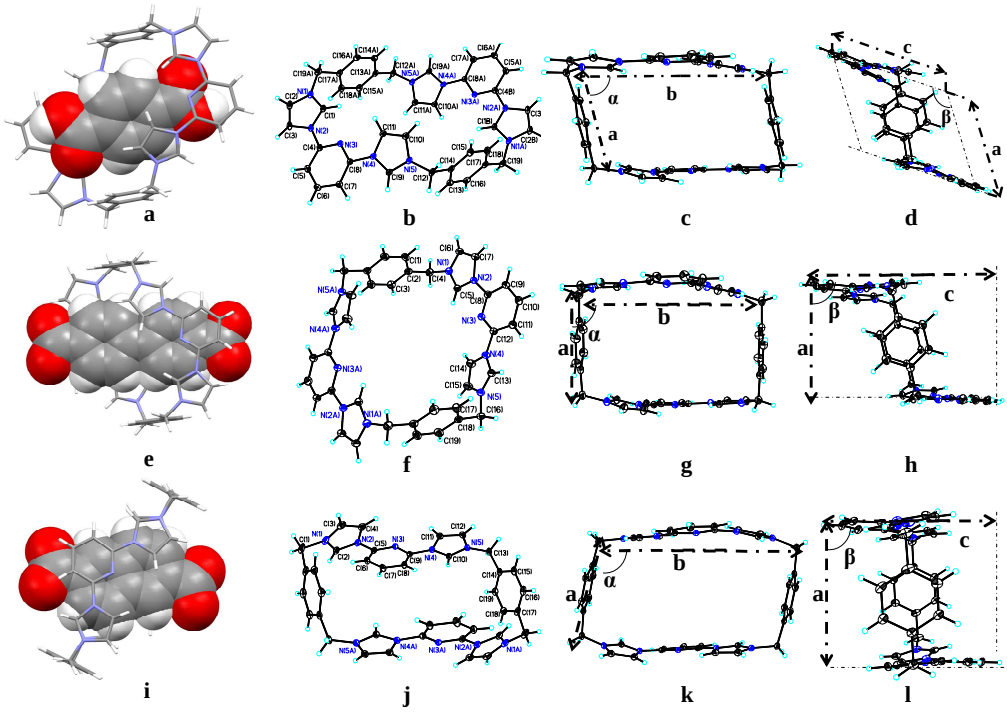

Figure S52. Comparitie analysis of the comformations seen in pseudorotaxane structures formed using macrocycle $\mathbf{1}^{4+}$. (a) Top view of the pseudorotaxane, (b) top view, (c) and (d) side views of the "part chair" conformation of $\mathbf{1}^{4+}$ in [$\mathbf{1}^{4+}$•**3**•3PF_6^-•4H_2O]. The important parameters of the cavities are listed as: Selected distances [Å] a = 5.818, b = 9.374, c = 5.900. Selected angles: α 103.16 º, β 120.00 º. (e) Top view of the pseudorotaxane as well as the top view (f) and side views (g) and (h) of the "complete chair" conformation of $\mathbf{1}^{4+}$ in [$\mathbf{1}^{4+}$•$\mathbf{7}_2$• 2DMF•7.5H_2O]. The important parameters of the cavities are listed as: Selected distances [Å] a = 5.826, b = 10.183, c = 9.812. Selected angles: α 92.63 º, β 120.00 º. Also, shown is the op view of the pseudorotaxane (i and j), as well as the side views (k) and (l) of the "regular box" conformation of $\mathbf{1}^{4+}$ in [$\mathbf{1}^{4+}$·**10**·10 H_2O]. The important parameters of the cavities are listed as: Selected distances [Å] a = 5.785, b = 11.598, c = 6.883. Selected angles: α 98.64 º, β 90.00 º.

References:

(1) Abelson, J. N.; Simon, M. I.; Carter Jr., C. W.; Sweet, R. M. Methods in Enzymology, 276: Macromolecular Crystallography, Part A, 307 – 326, Academic Press (1997).

(2) Altomare, A.; Burla, M. C.; Camalli, M.; Cascarano, G. L.; Giacovazzo, C.; Guagliardi, A.; Moliterni, A. G. G.; Polidori, G.; Spagna, R. *J. Appl. Cryst.* **1999**, *32*, 115-119.

(3) Sheldrick, G. M. SHELXL97. Program for the Refinement of Crystal Structures. University of Gottingen, Germany, 1994.

(4) Cooper, R. I.; Gould, R. O.; Parsons, S.; Watkin, D. J. *J. Applied. Cryst.* **2002**, *35*, 168-174.

(5) Farrugia, L. J. *J. Applied. Cryst.* **1999**, *32*, 837-838.

(6) $R_w(F^2) = \{w(|F_o|^2 - |F_c|^2)^2/w(|F_o|)^4\}^{1/2}$ where w is the weight given each reflection.

$R(F) = (|F_o| - |F_c|)/ |F_o|\}$ for reflections with $F_o > 4((F_o))$.

$S = [w(|F_o|^2 - |F_c|^2)^2/(n - p)]^{1/2}$, where n is the number of reflections and p is the number of refined parameters.

(7) Wilson, A. J. C. International Tables for X-ray Crystallography. Vol. C, Tables 4.2.6.8 and 6.1.1.4. Boston: Kluwer Academic Press (1992).

(8) Sheldrick, G. M. (1994). SHELXTL/PC (Version 5.03). Siemens Analytical X-ray Instruments, Inc., Madison, Wisconsin, USA.

(9) Riddick, J. A., Bunger, W. B.; Sakano T. K. Techniques of Chemistry 4th ed., Volume II. Organic Solvents. New York, NY: John Wiley and Sons. 1985.

(10) National Industrial Chemicals Notification and Assessment Scheme. Australia.

(11) Job, P. *Ann. Chim.* Paris, **1928**, *9*, 113-203.

(12) a) Connors, K. A. Binding Constants, John Wiley and Sons: New York, 1987. b) Hyperquad2003: Gans, P.; Sabatini, A.; Vacca, A. Talanta, 1996, 43, 1739-1753.

(13) a) Neuhaus, D.; Williamson, M. P. The Nuclear Overhauser Effect in Structural and Conformational Analysis; VCH Publishers; Cambridge, U. K., 1989. b) Friebolin, H. Basic One- and Two-Dimensional NMR Spectroscopy; WILEY-VCH, Weinheim, 2005.

(14) Martin, R.B. *Chem. Rev*. **96**, 3043-3064 (1996).

(15) *National Industrial Chemicals Notification and Assessment Scheme*. Australia.

(16) Gong, H.-Y.; Rambo, B. M.; Karnas, E.; Lynch, V. M.; Sessler, J. L. *Nature. Chem.* **2010**, *2*, 406-409.